E&TR

Energy and Technology Review
Lawrence Livermore National Laboratory
August 1982

MASTER

Briefs

A Universal Sensor for Potentiometric Titrations

The amount of a substance dissolved in a solvent can be measured by a technique called titration. To titrate a solution, we add, stepwise or continuously, a standardized reagent (the titrant), which reacts with the substance being measured (the analyte) to produce a chemical change when the substance has reacted completely. The point at which this change occurs is called the endpoint of the titration. In potentiometric titration, a technique used for several decades, the endpoint is signaled by a change in the electromotive force (potential) between two dissimilar electrodes, the sensor and the reference, immersed in the solution.

Depending on the ion being measured, various kinds of sensor are used to detect the endpoint of a potentiometric titration. In acid-base titrations, the electrodes are made of glass; in oxidation-reduction titrations, of gold or platinum. Ion-selective electrodes, developed more recently, are used to sense specific ions. The current cost of these specialized sensors ranges from $40 for an acid-base electrode to as much as $355 for a potassium-sensitive electrode. We have designed and tested a simple and inexpensive universal sensor that can be easily fabricated in the laboratory.

In 1970, it was reported that polyvinylchloride (PVC) membranes plasticized with dioctylphthalate (DOP) respond to some organic cations. Investigators recently used an electrode containing such a membrane to signal the endpoint in a very specific reaction, the titration of an alkyl aromatic sulfonate with quaternary ammonium ions. We have demonstrated that this type of sensor is applicable to a wide variety of potentiometric titrations: acid-base, precipitation, compleximetric, and oxidation-reduction. Table 1 lists some of the titrations that are feasible with this technique. The sensor can measure both organic and inorganic ions, its selectivity depending entirely on the interaction between the analyte and the titrant. Its versatility is limited only by the fact that the titration medium must be aqueous, as the membrane will dissolve in organic solvents.

To fabricate the sensor, we cut a rod 15 cm long from a standard 30-cm graphite spectroscopic rod 6 mm in diameter. We prepared the coating solution by dissolving 1 g of low-molecular-weight PVC and 1 g of DOP in 30 ml of tetrahydrofuran. We coated the graphite rod to a depth of 1.3 cm by dipping it for a few seconds into the coating solution and air drying it. The process

Table 1 Some feasible potentiometric titrations using a graphite sensor coated with PVC-DOP (Roman numerals indicate valence state).

Ion measured	Titrant	Titration type
Perchlorate	Cetylpyridinium	Precipitation
Hexafluorophosphate	Cetylpyridinium	Precipitation
Peroxydisulfate	Cetylpyridinium	Precipitation
Nitroform	Cetylpyridinium	Precipitation
Picrate	Cetylpyridinium	Precipitation
Tetraphenylborate	Cetylpyridinium	Precipitation
Dodecylsulfate	Cetylpyridinium	Precipitation
Thallous	Tetraphenylborate	Precipitation
Bromide + iodide	Silver (I)	Precipitation
Fluoride	Lanthanum (III)	Precipitation
Tungstate	Lead (II)	Precipitation
Acid phthalate	Sodium hydroxide	Acid-base
Ferrous	Chromate	Oxidation-reduction
Ethylenediamine tetraacetate	Lead (II)	Compleximetric

Table 2 Performance of various graphite sensor materials coated with PVC-DOP. Approximately 35% nitroform in solution was titrated with 0.05 N cetylpyridinium chloride.

Material	Number of tests	Nitroform recovered, mean %	Standard deviation	Endpoint break, mV
Spectroscopic graphite[a]	3	35.58	0.02	180
Mechanical-pencil "lead" in glass capillary[b]	4	35.94	0.06	110
Pencil[c]	4	35.74	0.03	30

[a]Cost $1.29 each.
[b]Turquoise Eagle drawing lead; cost $0.07 each.
[c]No. 2 Astro 155 Bondexed lead pencil; cost $0.04 each.

was repeated three or four times. (The cost of the coating solution was less than $0.01 per electrode; one batch of the PVC-DOP solution will coat many electrodes and will keep indefinitely in a stoppered glass bottle.) We then connected the coated rod to a potentiometer. Any single-junction electrode can serve as the reference electrode; we used a silver-silver chloride reference containing a salt bridge of 0.1 N sodium nitrate.

It has been conjectured that the sensitivity of such electrodes may result from the formation of freshly precipitated complex compounds on the membrane during titration. These precipitated compounds gradually saturate the plasticizer in the membrane. The steepness and magnitude of the potential break at the endpoint is governed by the solubility product (the equilibrium between ions and solids in solution) of the precipitated species and is also influenced by the plasticizer in the membrane.

Although this explanation no doubt applies to precipitation titrations, it fails to account for the endpoints in other types of potentiometric titration we have investigated. We surmise that in acid-base, oxidation-reduction, and compleximetric titrations, an electrode may undergo a potential change when a major change occurs in the ionic composition of the solution.

As a demonstration of the versatility of our technique and as a technical *tour de force*, we measured nitroform (a water-soluble organic compound) in solution by titrating it with cetylpyridinium chloride, using the following electrode materials coated with PVC-DOP:

1. Standard spectroscopic graphite.

2. A graphite "lead" from a mechanical pencil crimped into a glass capillary for mechanical strength.

3. A No. 2 wooden pencil.
In the last, we pried the eraser loose and filled the cavity with solder to make electrical contact with the graphite core (Fig. 1).

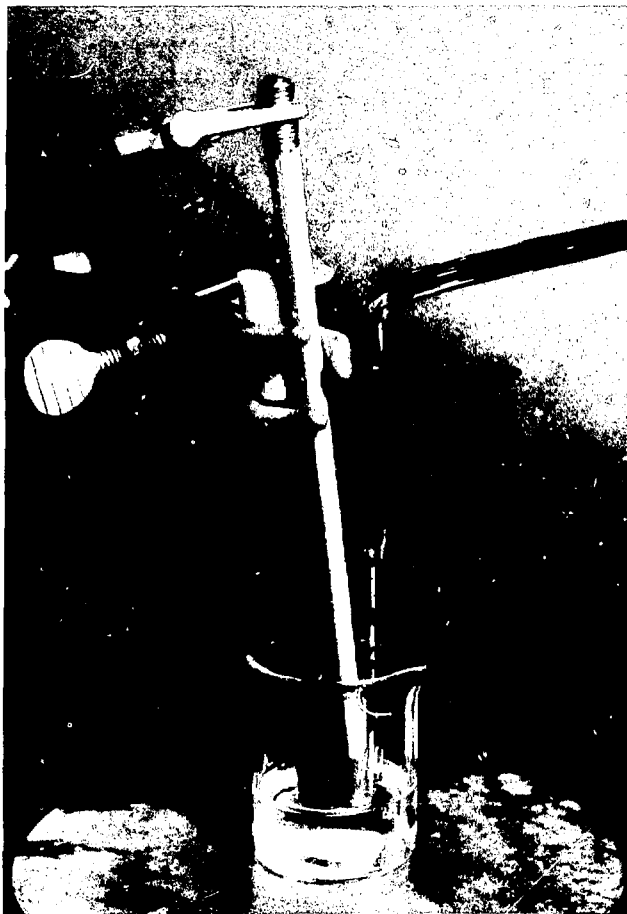The results, shown in Table 2, indicate acceptable precision in all cases (endpoint breaks were smaller with the

Fig. 1

A universal potentiometric sensor. The sensor electrode, coated with PVC-DOP, is a standard No. 2 graphite pencil.
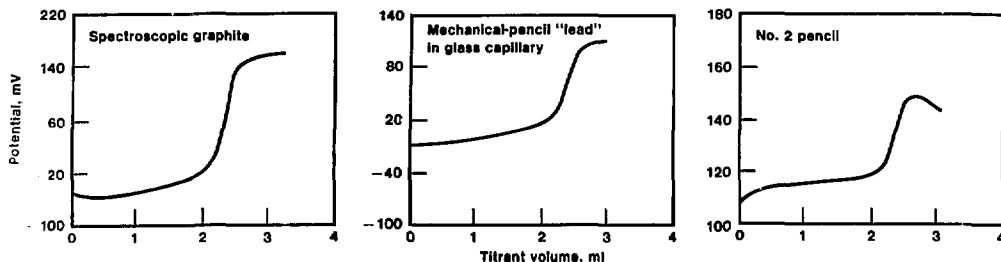
Fig. 2

Titration curves for approximately
35% nitroform solution titrated with
cetylpyridinium chloride; three graph-
ite materials were used for the PVC-
DOP-coated sensor electrode.

second and third variants). Figure 2
shows the corresponding titration
curves. The electrode material for the
second variant cost $0.07 and for the
third $0.04. Though we do not advocate
regular use of these two materials, we
have demonstrated that in some appli-
cations it is possible to do the research

and write up the results with the same
pencil.

For further information contact
Walter S. Selig (415) 422-6378.

Successful Demonstration
of the AVLIS Process

We recently performed the first
uranium enrichment demonstration
using lasers in which both the isotopic
reduction in the input and the isotopic
enrichment of the product were
measured. The experiment was an inte-
grated test of the Atomic Vapor Laser
Isotope Separation (AVLIS) process de-
veloped at LLNL and recently selected
by the Department of Energy for large-
scale development. The enrichment and
mass balance indicated by the isotopic
analysis of the product and of the tails
matches our expectations based on the
AVLIS process model and gives us
added confidence that our plant-
performance projections are accurate.

The three basic steps of the AVLIS
process (Fig. 1) are as follows:

• An electron-beam heats a crucible
of molten uranium metal to produce a
sheet-like stream of atomic uranium
vapor.

• The atomic vapor flows into a
separation zone where it encounters
pulsed laser beams. These lasers, tuned
precisely to visible-light transitions of
uranium-235, selectively photoionize
the uranium-235.

• Electromagnetic fields draw the
ions onto charged-product collector
plates, leaving the bulk of the vapor to
accumulate on a tails collector plate.

Enrichment performance is measured
in terms of conventional separative
work units (SWUs), a value function re-
lated to the energy required to separate
or unmix a feed stream of specified as-
say into product (enriched) and tails
(depleted) streams, also of specified as-
says. In the case of light-water reactor
(LWR) fuel, these assays are a 0.7%
uranium-235 feed, 3.2% uranium-235
product, and 0.25% uranium-235 tails.

For the AVLIS process, the separative
work performance is described
conveniently by two key process
parameters—the stripping efficiency η_s
and the nonselective pickup ϕ. The
stripping efficiency is the fraction of
uranium-235 in the feed stream that is
ionized by the laser and collected on
the product plates; it is the product of
three main factors—available atom
population fraction, photoionization ef-
ficiency, and extraction efficiency. Strip-
ping efficiency determines the tails as-
say and strongly impacts the separative
work performance.

The nonselective pickup ϕ is the frac-
tion of the feed stream that is deposited

Fig. 1

Essential elements of the AVLIS process.
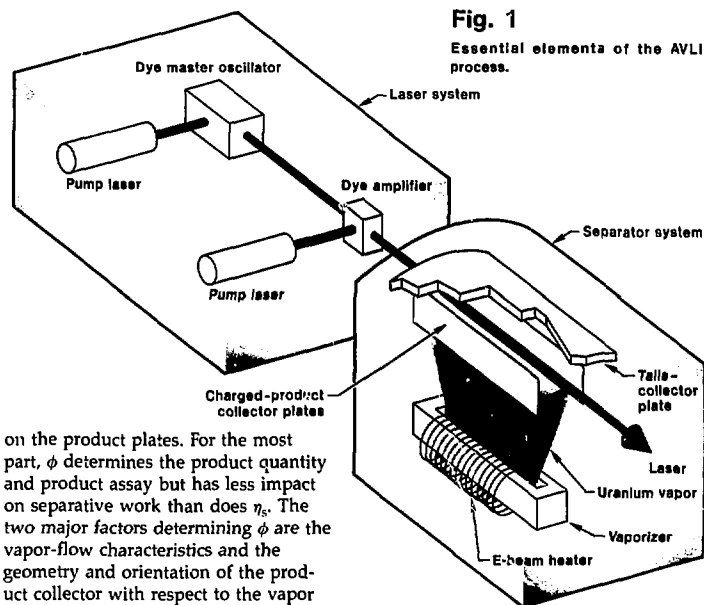
on the product plates. For the most part, ϕ determines the product quantity and product assay but has less impact on separative work than does η_s. The two major factors determining ϕ are the vapor-flow characteristics and the geometry and orientation of the product collector with respect to the vapor stream. In previous experiments designed to isolate the controlling effects, we extensively studied the separate factors that determine η_s and ϕ. The results of these experiments provided the basis for our understanding of the process and allowed us to model and project AVLIS plant performance.

Our recent enrichment demonstration was designed to simulate as closely as possible full-scale plant operating conditions and thus provide a benchmark for the process models that predict the integrated system performance. Although the available laser and vapor facilities are at smaller scale than the full-scale plant, we were able to duplicate the most important features of photoionization and ion extraction in a plant-geometry extractor cell at plant vapor density and laser fluence.

The experiment yielded high-quality data. From the overall weights and assays, we were able to determine the average ϕ within ±1% and the average η_s within ±8%. From the weight and assay distributions and from measurements of the vapor properties and total charge collected during the experi-

ments, we were able to make detailed comparisons between the model predictions and measured values for the separate factors that determine the overall performance. When scaled to plant conditions for such factors as full laser repetition frequency (the experiment was done at approximately one quarter the plant laser repetition rate), the measured stripping efficiency is consistent with the baseline plant design and model predictions for the separate performance factors in the experiment. Additional scaling factors to which this enrichment experiment was not sensitive were tested in a recent set of complementary experiments.

As we proceed to large-scale testing of the process, we will continue to perform enrichment demonstrations not only to show that the separate AVLIS subsystems can be successfully integrated but also to refine our model predictions for plant performance.

For further information contact Robert L. Woerner (415) 423-1868.
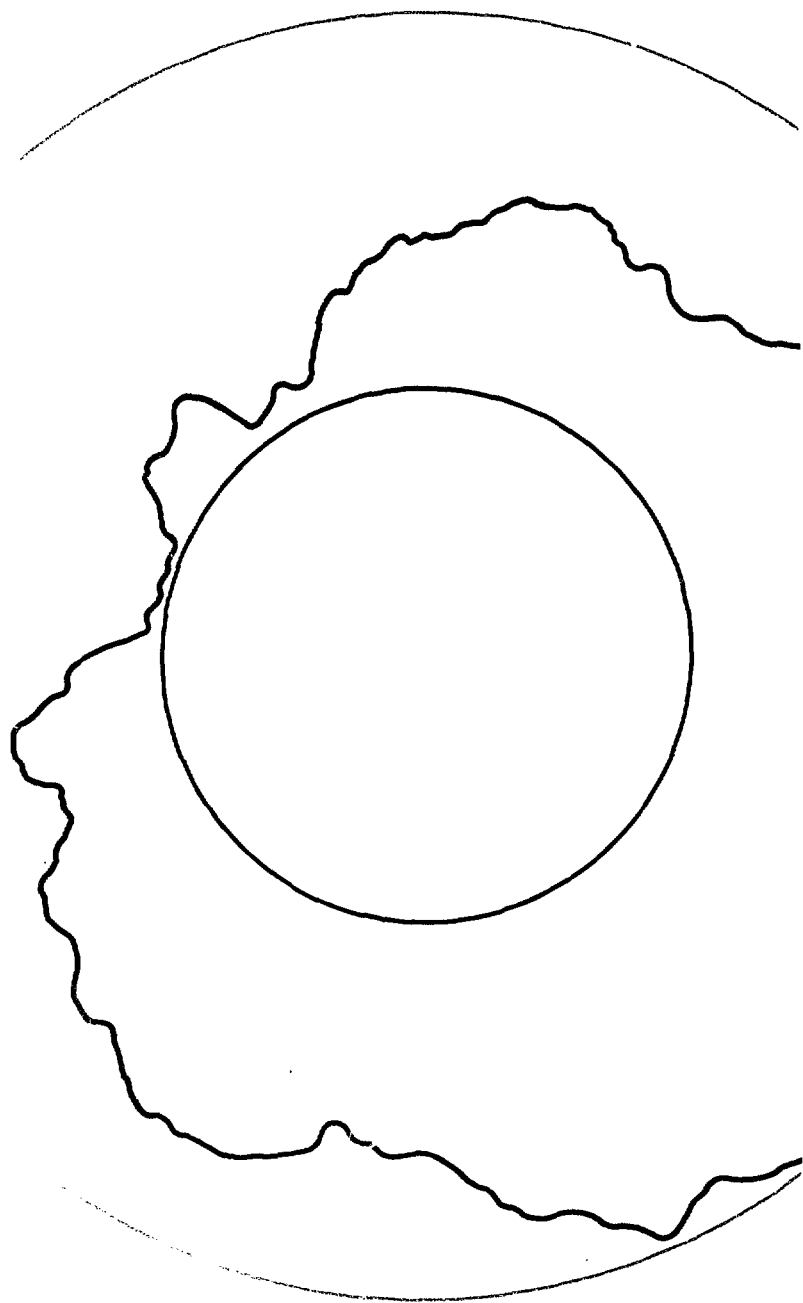
The Compuron:
How Round
is Round

We have applied microcomputer technology
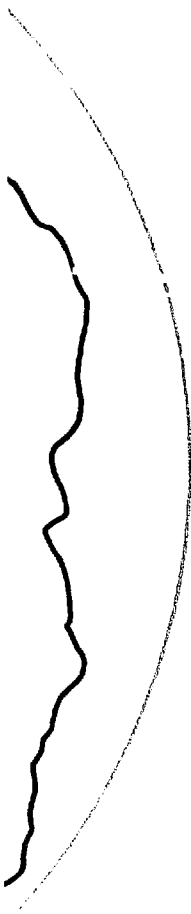to the task of inspecting machined parts to
develop an ultraprecise roundness gauge.

Certain devices, such as ultraprecise
gyroscopes and implosion systems, per-
form better and better the more nearly
they approach perfect roundness. In
some applications, minor deviations
from roundness may be tolerated so
long as we can measure precisely their
magnitude and location. In others, it is
important to measure precisely the fre-
quency distribution of deviations from
roundness. In all these cases, the more
accurately we can measure the shape,
the more reliably the scientists and
their computers can predict how the
device will perform.

Until recently, advances in precision
machining had outstripped our ability
to measure departure from roundness,
especially in the matter of the fre-
quency distribution. Our diamond turn-
ing and lapping machines had pro-
duced parts that were perfectly round,
according to our best measurements,
and yet the performance showed that
there were undetected deviations. Evi-
dently, there was a need for inspection

(a) **(b)**

Roundness error

Polar chart center ⌐

MRS center ⌐

Trace of perfect part with excessive eccentricity (limacon shape) ⌐

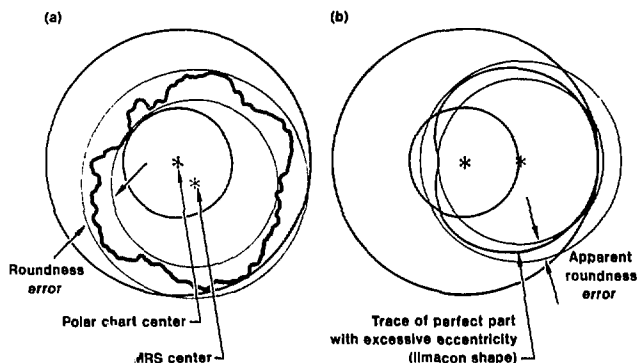Apparent roundness error

Fig. 1

Assessment of roundness (or, more accurately, out-of-roundness). In the minimum-radial-separation (MRS) method (a), an operator uses a transparent template of concentric circles and a center hole to find the MRS center, *which gives the minimum value for* the difference in circle radii and, hence, the roundness error. The distance between the MRS and polar chart centers represents the eccentricity of the part on *the rotating table* (and thus is not a roundness error). An attractive feature of the MRS method is that this eccentricity error can be eliminated, simplifying the task of centering "perfectly" the part on the rotating table. However, eccentricity still must be held below the roundness error or a second-order *limacon error* will result. As shown in (b), if even a perfectly round part is too eccentric, an apparent roundness error will be measured.

instrumentation of improved accuracy and precision.

The deviations from roundness that concern us here are extremely small, less than a tenth of the wavelength of visible light, but they can make a measurable difference. At present, the need for roundness measurements to this degree of accuracy is limited to high-technology areas. As precision machining technology spreads into the broader market place, however, the need for accurate inspection processes will surely follow.

How do we define roundness? Or more precisely, since by "roundness" we are really speaking of "deviations from perfect roundness," how do we define (or measure) the nonroundness of a nonround part? In fact, several methods are recognized, all of which employ concentric circles but differ as to how the center point is located.

One way this is done is shown in Fig. 1. By enclosing the polar part trace between two concentric circles, we can locate the common center to yield a minimum value for the roundness error. This method, called minimum radial separation (MRS), is attractive for analogue instruments because an inspector can learn to locate the MRS center reasonably quickly using a transparent template with many scribed concentric rings and a center hole. However, the MRS method is not mathematically rigorous: certain part profiles can have more than one MRS center, and the roundness value thus

Sources of Error

Roundness measurements suffer from two broad categories of error, instrument errors and data-reduction errors. Instrument errors can be subdivided into repeatable and nonrepeatable errors.

Repeatable errors occupy an important niche in precision-engineering applications, in that they often can be eliminated through self-proving tests. The dominant source of repeatable errors in measurements of roundness is movement of the spindle and part toward or away from the gaugehead as a function of the angle of rotation, due to geometric imperfections in the air-bearing components. This is known as radial-motion error, and it adds to the roundness-error signal coming from the part surface itself.

These two signals can be separated and identified, however, by making a second measurement with the part and gaugehead reversed relative to the spindle (indexed 180 deg). This self-proving technique (described in Ref. 1) is analogous to a carpenter checking his bubble level by reversing it 180 deg on the same work surface. With a computer-based system, removal of radial-motion error is straightforward. The profile can be stored in memory and then simply subtracted from the measured profile.

Because repeatable errors can be eliminated (rather easily with a computer-based system), the accuracy of roundness measurements is limited ultimately only by nonrepeatable errors. Nonrepeatable instrument errors include mechanical deflections between the part and the gaugehead, caused by vibration, force variations, or thermal disturbances, as well as by electronic noise. Mechanical sources can be internal, such as spindle drive train imbalances, or external, such as seismic or acoustic vibrations. Where these errors are sufficiently random with respect to spindle rotation, multiple-revolution averaging can be used to reduce the effects of nonrepeatable errors; this is readily accomplished with a computer-based system.

Data-reduction errors are a much larger problem with analogue data interpreted from a polar chart by an inspector than for a computer-based system. These errors arise from the linearity and dynamic response characteristics of the polar recorder, human errors in constructing the concentric circles, and problems of accurate interpretation due to noise, finite line widths, etc. Also, there is no reasonable method for removing the limacon error due to inadequate part centering (see Fig. 1). To eliminate these errors (as far as is practical), the usual procedure is to provide the inspector with guidelines for maximum eccentricity so that inadequate measurements can be repeated with better centering.

When, however, computerized data reduction and analysis are available, the limacon distortion can be seen to consist of the first-order terms of the harmonic analysis of the waveform. These terms can be calculated and removed with the aid of fast Fourier transform (FFT) routines (see figure below).

All things considered, the system accuracy of an analogue instrument can be expected to fall in the range of 50 to 250 nm, with the greater accuracy achieved only by paying careful attention to eliminating human errors. To obtain further improvements in accuracy, a digital, or computer-based, system of roundness measurement is the logical development.
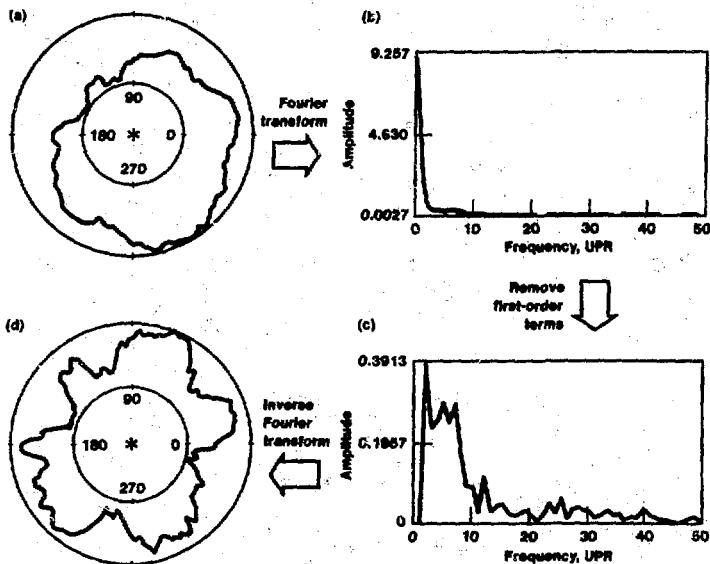
A digital method for removing the error caused by miscentering of the part and for locating the root-mean-square part center. Shown in (a) is the tracing obtained from the off-center part. Harmonic analysis of this off-center tracing (b) reveals the predominance of first-order (low-frequency) terms corresponding to the limacon error. In (c) we show the same spectrum with the first-order terms removed. Because of the increased magnification made possible by suppression of the first-order terms, the higher-frequency terms become apparent. The roundness trace in (d) illustrates the result of the correction for the centering error.
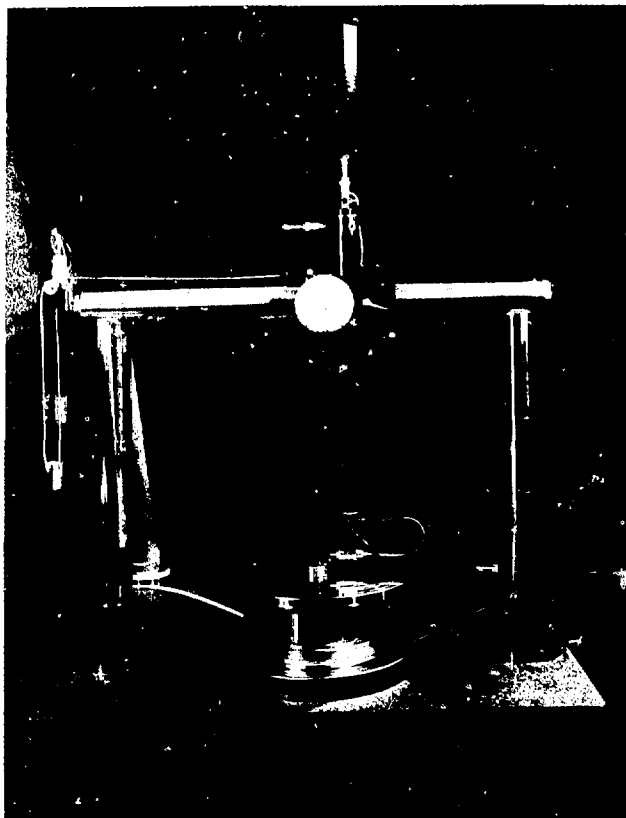
Fig. 2

An early version of the Compuron. This instrument is of the rotating-spindle type and can accommodate parts 400 mm in diameter, 350 mm long, and weighing up to 225 kg. Its accuracy goal is 2.5 nm, with a resolution of 0.25 nm. The Compuron is linked to a microcomputer system that makes operation of the instrument, after centering of the part to within the gauging range and initial input of desired parameters, completely automated.
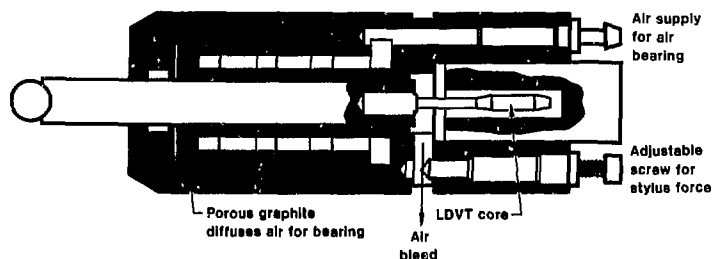
Roundness Measuring Instruments

Conventional roundness-measuring equipment consists of two key parts: a spindle to hold the part being measured and a gaugehead with a stylus for measuring roundness deviations of the part surface. In some devices, the spindle rotates and the gaugehead is stationary; in others, the part is stationary and the gaugehead revolves around it. In either case, the output of the gaugehead amplifier drives the pen of a polar chart recorder that turns synchronously, producing a highly magnified map (typically about 50 000×) of the peaks and valleys on the part surface (at the particular plane traced out by the gaugehead's stylus).

With a good instrument and a skilled operator, the typical total error for roundness measurements with a conventional analogue instrument is on the order of 50 to 250 nm. Some improvement is possible, in some instruments, by a "reversal technique" that compares the results of two roundness measurements taken one after the other.[1] In both measurements, the starting point of the stylus on the workpiece remains the same, but in one measurement both the workpiece and the gaugehead have been turned 180 deg with respect to the spindle. With a conventional analogue device, however, limitations imposed by trace distortion and the difficulty of interpretation make it impractical to improve the accuracy beyond the 25-nm level (see box on p. 2).

The LLNL Compuron

Since no two inspectors, no matter how highly trained, can agree exactly on the interpretation of analogue data, one obvious recourse is to call in the computer. For a given set of data, a computer program can be relied on to yield the same interpretation, time after time. Therefore, the only remaining problems are to obtain the best possible data, to convert the data into a form the computer can use, and to be sure that the program causes the computer to analyze the data correctly.

determined depends, to an extent, on the magnification of the part trace.

Another method, which we have used with the LLNL Compuron roundness measuring instrument, is a least-squares best-fit of the center which is unique and insensitive to the level of magnification used. Having located this best-fit center we can measure roundness deviations with respect to the center. Although the least-squares method involves far too much manual calculation for an inspector using a polar chart, it is readily accomplished with Compuron's microcomputer data-acquisition system.

4

Air supply
for air
bearing

Adjustable
screw for
stylus force

Porous graphite
diffuses air for bearing

LDVT core

Air
bleed

Fig. 3

Construction details of the gaugehead assembly, showing the air bearing that permits the stylus force to be adjusted to less than 100 mg. The adjustable screw controls the air bleed (and hence the pressure) from the back chamber, thereby controlling the stylus force.

Computer-assisted precision measuring instruments are becoming more readily available commercially. For roundness measurements, there exists a computer-based, revolving-stylus instrument with an accuracy, in the frequency range from 1 to 20 UPR (undulations per revolution), of 5 nm in amplitude. However, rather than modify this instrument, we decided to develop our own in order to meet our specific accuracy needs and to accommodate large part sizes.

In metrology, it is desirable, though not always possible, to make every gauge ten times more accurate than the variations it is designed to measure. Since the diamond turning, polishing, and lapping techniques in use at LLNL are capable of producing parts round to 25 nm, we set the Compuron's accuracy goal at 2.5 nm. We also decided that the Compuron would be of the rotating-spindle type and be capable of accommodating parts 400 mm in diameter, 350 mm long, and weighing up to 225 kg, and of rotating them at 10 rpm. We specified that the minimum stylus force must be less than 100 mg, the maximum display magnification must be ten million, and the frequency cutoff at full accuracy must be at least 500 UPR, with the possibility of going up to 1500 UPR at reduced accuracy. (The former accuracy figure is based on LLNL needs; the latter stems from an ANSI standard calling for a 1500-UPR range.[3])

Figure 2 shows an early version of the LLNL Compuron. The support frame for the gaugehead is bolted directly to the granite base slab, which rests atop four self-leveling pneumatic vibration isolators. Computer modeling of this structure, during design, determined that the first resonant vibration mode is at 120 Hz, well outside the normal, 50-UPR operating range of the instrument at the standard spindle speed of 10 rpm.

Capstan drives give us coarse control over the vertical and horizontal position of the gaugehead. For fine adjustments (to the few-nanometre level), we use a combination of flexures and differential micrometers.

The gaugehead itself is a linear variable differential transformer (LVDT) developed at the Laboratory (Fig. 3), in which the sensing element floats on an air bearing. The air bearing eliminates dry friction in the gaugehead and allows us to adjust the stylus force to below 100 mg.

The rotary table holding the spindle also floats on an air bearing and is turned by a small variable-speed motor linked to it by a thin Mylar belt. The exact speed of rotation is of minor importance: a 4096-segment rotary encoder, attached to the bottom of the rotary table, triggers the data sampler at the proper intervals regardless of rotation speed.

The Computer

The Compuron is integrated with a microcomputer system (Fig. 4), which includes a graphics terminal, a hardcopy unit, and both hard- and floppy-disk drives. A 12-bit analogue-to-digital converter monitors the output of the LDVT's amplifier for input to the computer, and a four-pole Bessel filter ensures that the data sampling rate exceeds the frequency response of the
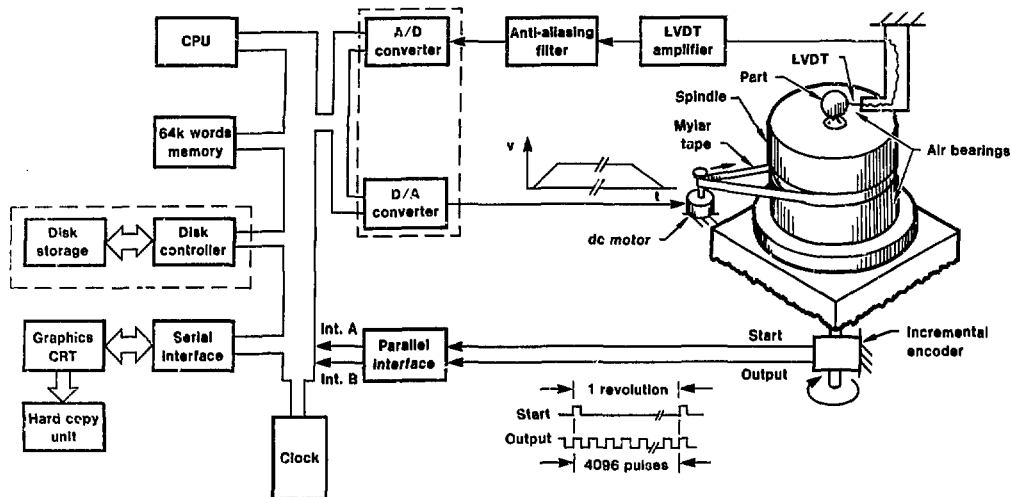
Fig. 4 Function diagram illustrating the integration of microcomputer hardware with the mechanical measuring equipment of the Compuron.
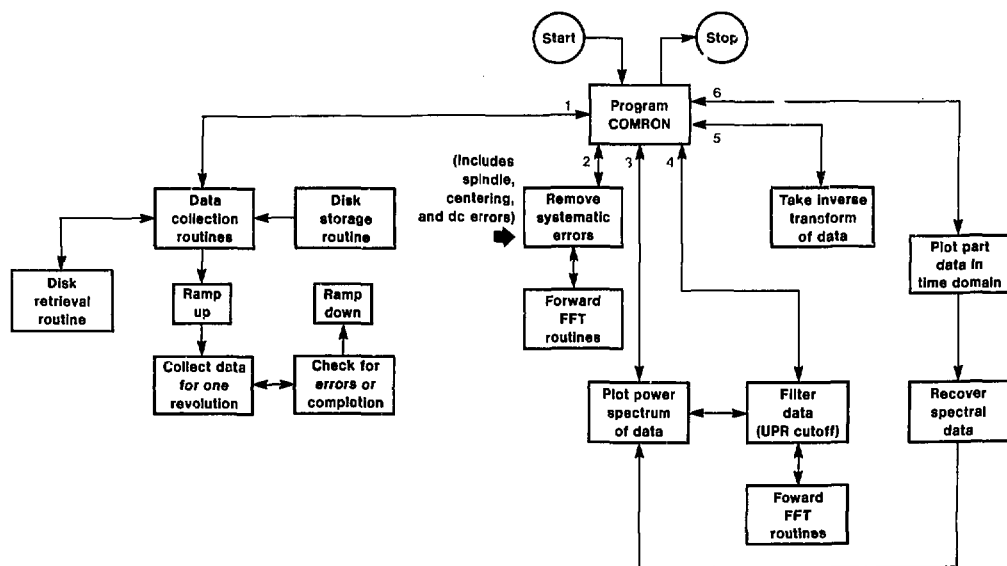

Fig. 5 Structure of the supporting software that automates the operation of the Compuron. Numbers around the program box denote the sequence in which the various operations occur.

amplifier by a factor of at least two. Even the spindle drive motor is under computer control.

The software for this system was written especially to make operation of the Compuron as straightforward and simple as possible. It consists of 44 Fortran routines (and one assembly-language routine for data acquisition) that control all aspects of information input, process control, and data reduction (Fig. 5). All the major routines are loosely coupled so that any of them may be modified without drastic effects on the other modules.

Furthermore, generous use of prompts enables even a relatively un-skilled operator to use the system effec-tively. Operation of the instrument, after rough centering of the part to within the gauging range of the instru-ment and initial input of desired parameters, is completely automated. Output, either of part roundness or har-monic analysis, appears first on the video display terminal and may then be printed at magnifications of up to ten million. The raw data may also be stored on floppy disk for future reference.

In addition to minimizing sources of system noise by seismic isolation and by careful electronic design, we also apply statistical methods. Our equip-ment can average the roundness data from up to 16 successive rotations to re-duce system noise effects by about 75%. To demonstrate this, we ran a test with the gaugehead capped (stylus im-mobilized relative to the LVDT hous-ing) to record system noise alone. The noise in one revolution was equivalent to a roundness error of 1 nm; when the noise was averaged over 16 revolutions the system error was reduced to 0.25 nm.

Another source of nonrepeatable errors is thermal drift, which in the un-regulated environment of a normal workroom can be as much as 1000 nm over a period of days. Over the period of a single revolution (6 s), however, the drift is generally tolerable. The soft-ware automatically considers 4097 data points in each revolution (the 4097th point is really the first point of the next revolution) and rejects the first 4096 points for excessive drift if the 1st and 4097th points fail to agree within a pre-scribed limit set by the operator (typi-cally 2.5 nm). The typical net drift of data averaged over 16 revolutions is less than 0.5 nm.

As mentioned in the box on error sources (p. 2), the reversal technique makes it possible to separate part and spindle errors. With our Compuron, it is unnecessary to repeat this procedure for subsequent measurements at the same axial location. The previously determined spindle error, stored on disk, may simply be subtracted automatically.

The only real limit to the accuracy of a metrology instrument is its repeatability.

Digital Filtering

Although our instrument can make measurements to 500 UPR (and up to 1500 UPR at reduced accuracy), for many purposes such a part trace is un-necessarily detailed. We do not need to modify the instrument to make mea-surements at lower UPR levels, how-ever. We can achieve the same result much more efficiently with digital filtering.

Digital filtering is a computer tech-nique that modifies the frequency dis-tribution of a set of data in a specified fashion by simulating the effect of a frequency filter. For our purposes, we simulate a low-pass filter, one that cuts

Fig. 6

An example of digital filtering. (a) A roundness trace with an upper frequency limit of 200 UPR. (b) The frequency spectrum of this trace (same as c in the box on p. 2). (c) The spectrum after suppression of frequencies above 20 UPR. (d) The resulting smoothed trace.
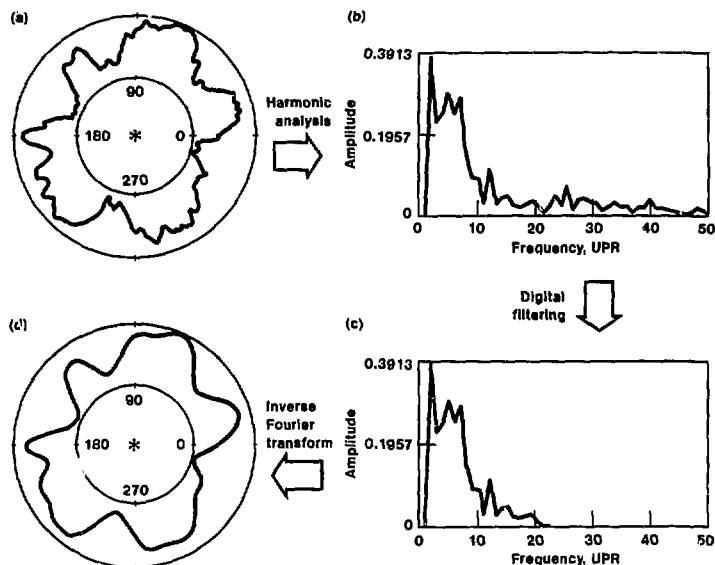
off frequencies above a selected maximum. The characteristics of the Compuron that make this technique possible are:

- The use of the Fourier transform in the harmonic analysis.
- The large number of data points per revolution (4096), which ensures that the low-frequency components are adequately defined.
- The storage of the raw data on disk, which permits the computer to manipulate copies of the data to provide output at any number of different UPR values.

Figure 6 illustrates the process, starting with a roundness trace at 200 UPR (a) and its frequency distribution (b). Application of the digital filter removes frequencies above 20 UPR (c). The inverse of the Fourier transform produces the smoothed roundness trace (d).

Results

The only real limit to the accuracy of a metrology instrument is its repeatability. Errors that are repeatable are presumably measurable, and therefore susceptible to electronic or mechanical compensation. The unrepeatable errors are the ones that cause problems.

To assess the repeatability of the whole system, we took a series of measurements on a representative steel ball. Figure 7a shows a repeatability measurement consisting of the difference between two 16-revolution averages with a 50-UPR cutoff taken about 30 min apart. The maximum peak-to-valley amplitude is 0.75 nm with a root-mean-square value of 0.25 nm.

Repeatability over a longer period (hours or days) deteriorates to about 1.3 to 2.5 nm. This is hardly surprising, however, since we are still operating the instrument in a workroom with minimal temperature control. The observed temperature fluctuations are enough to distort the spindle housing and change the spindle radial motion.

We assessed the overall accuracy of the instrument by first using the reversal technique to establish and store the spindle error, and then making a series of measurements of a master gauge ball oriented at different angular positions relative to the spindle. We took the instrument accuracy to be the largest

deviation between any two error-corrected traces. Figure 7b shows two 16-revolution averages with a 50-UPR cutoff taken about 60 min apart. The maximum peak-to-valley amplitude is 2.5 nm, the claimed accuracy of the instrument.

Applications

A new test of Einstein's General Theory of Relativity, involving the precession of a superconducting gyroscope in polar orbit about the earth, has recently become possible because of advances in manufacturing and measuring technologies. The heart of this instrument will consist of a rotating sphere of superhomogeneous fused quartz coated with a thin layer of superconducting metal. The instrument is being developed at Stanford University for launch by the Space Shuttle.[4]

Existing technology makes it possible to maintain the gyroscope at liquid-helium temperatures for more than a year, to reduce external torques and accelerations to the necessary incredibly low levels, and to read out the precession of the gyroscope with reference to the fixed stars. The remaining difficulty is in guaranteeing the sphericity of the gyroscope ball to 10 nm. We have been asked to assist this project by performing the necessary measurements with our Compuron.

In our own programs, our measurements give LLNL scientists information never before available on the frequency distribution of departures from roundness in implosion systems. This information is particularly valuable because it is already in a form suitable for input to their computer codes for modeling implosions. This new information potentially reduces a significant source of uncertainty in their modeling predictions.

Future Development

Although we have met our original accuracy goal, further improvements are possible. For one, we can greatly reduce the error from thermal drift by maintaining the surrounding air at constant temperature. We are designing a laminar-flow enclosure to maintain the air temperature at 20 ± 0.005°C.

(a)

90
180 ✱ 0
270

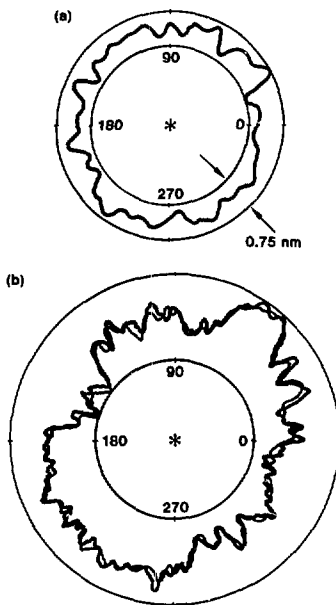0.75 nm

(b)

90
180 ✱ 0
270

Fig. 7

Measurements of accuracy and repeatability. (a) The difference between two roundness measurements (each the average of data for 16 revolutions) on the same workpiece taken about 30 min apart without disturbing the part in the spindle (repeatability). (b) The difference between two roundness measurements (each the average of data for 16 revolutions) on the same workpiece taken about 60 min apart, with the part rotated in the spindle. The maximum deviation between the two traces is only 2.5 nm.

Also, we have detected seismic coupling between the instrument and the floor through the leveling valves on the pneumatic isolators. We are currently developing air-bearing spool-valve replacements. When these are perfected and installed, they should substantially reduce the random motion due to structural vibration.
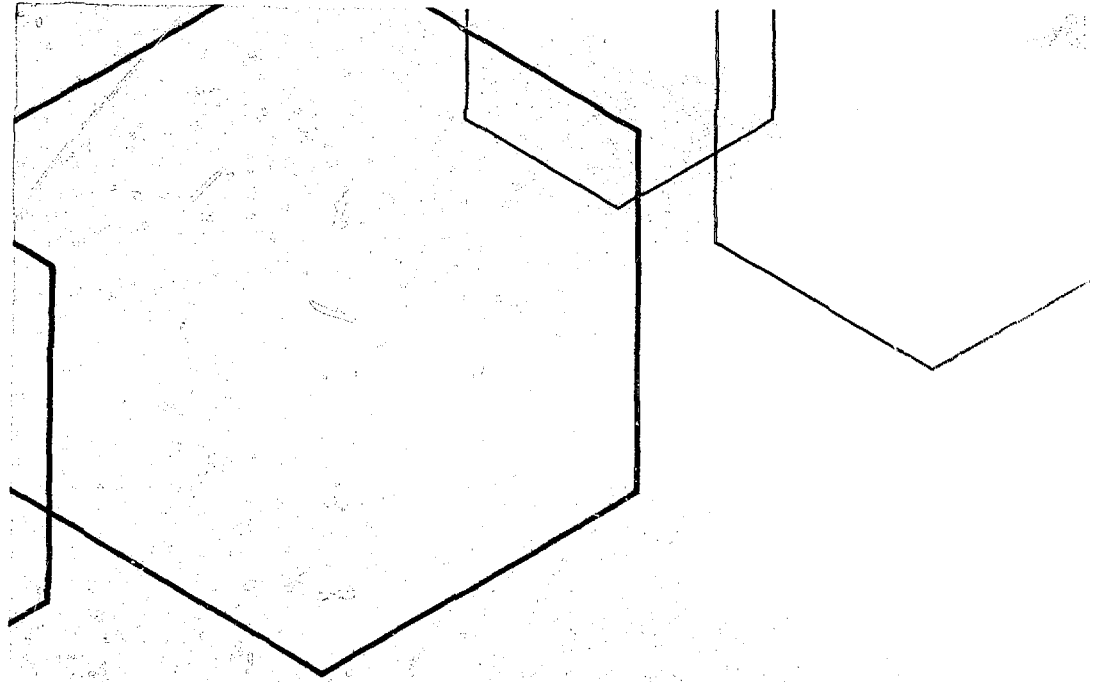
With these improvements, the accuracy of our Compuron will be improved, possibly even to 1.25 μm.

Key Words: Compuron; computer-assisted inspection; fast Fourier transform; harmonic analysis; metrology; relativistic gyroscope experiment; roundness measurements.

Notes and References

1. R. R. Donaldson, *Ann. CIRP*, 21, 1 (1972).
2. D. G. Chetwynd and G. J. Siddall, *J. Phys. E: Sci. Instrum.*, 9, 537 (1976).
3. American National Standards Institute (ANSI), "Measurement of Out-of-Roundness," Standard 889.3.1-1972 (1972).
4. C. W. F. Everitt, J. A. Lipa, and G. J. Siddall, *Precision Engineering*, 1(1), 5 (1979).
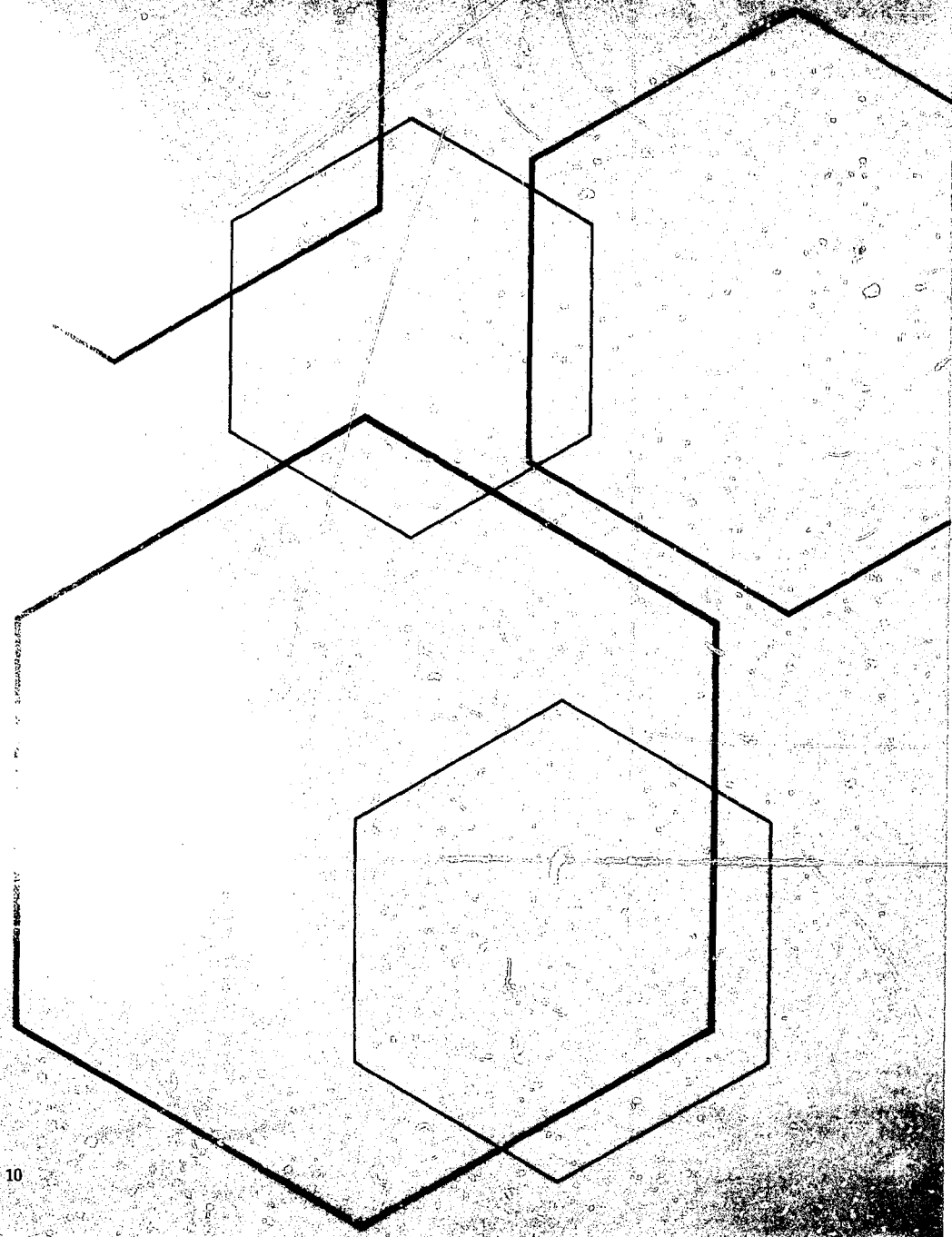
Electrosynthesis of N₂O₅: the Key to Inexpensive HMX

We have further developed an electrolytic technique for preparing dinitrogen pentoxide. This process is a potentially less expensive step in the large-scale synthesis of the explosive HMX.

The cyclic nitramines RDX and HMX, two crystalline explosives that came into prominence during the 1940s, have by now become the key ingredients in all high-energy munitions and in an increasing number of rocket propellants (e.g., for the Trident and MX missiles). HMX offers substantial advantages over RDX, not only in thermal stability but also in its higher density, which permits it to deliver more energy per unit volume. Unfortunately, HMX is more difficult to produce than RDX and therefore is substantially more expensive (approximately $7/kg for RDX and $22/kg for HMX).

Fig. 1

(a)

Hexamine

(b)

Hexamine $\xrightarrow{100\% \ HNO_3}$ RDX

(c)

Hexamine $\xrightarrow{NH_4NO_3, \ HNO_3 \atop Ac_2O, \ AcOH}$ RDX + HMX

(d)

Hexamine $\xrightarrow[H_2SO_4, \ HNO_3, \atop Ac_2O]{Step \ 1}$ DADN $\xrightarrow[N_2O_5]{Step \ 2}$ HMX
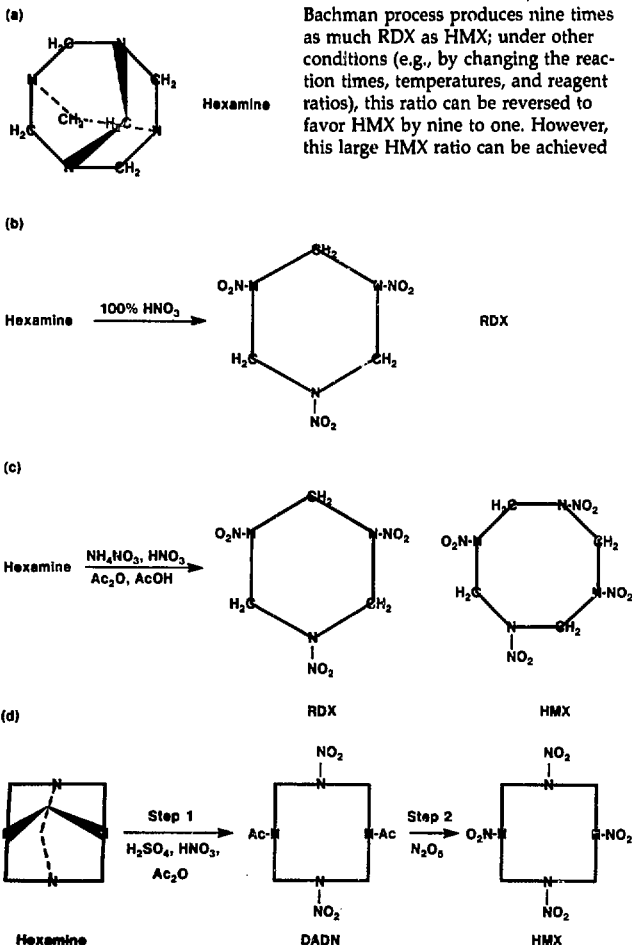
Production of either RDX or HMX begins with hexamine (Fig. 1a). In many countries, RDX is made by the Woolwich reaction (Fig. 1b), which involves reacting hexamine with fuming nitric acid (HNO_3). In the United States, RDX is produced by the Bachman process, a multistep procedure that reacts hexamine with nitric acid and ammonium nitrate in acetic acid and acetic anhydride and gives a mixture of RDX and HMX (Fig. 1c).

Under normal conditions, the Bachman process produces nine times as much RDX as HMX; under other conditions (e.g., by changing the reaction times, temperatures, and reagent ratios), this ratio can be reversed to favor HMX by nine to one. However, this large HMX ratio can be achieved only at the expense of a significant reduction in overall yield and throughput. These factors, together with the need to separate and purify the HMX, make it three to five times as expensive as RDX. At present, however, this is the only available method for producing HMX.

Since HMX is the more desirable material, there is a need for an inexpensive process that yields HMX alone. Such a process would release HMX from its dependence on RDX and make U.S. nitramine production more flexible. This goal provides the incentive for research on new synthetic routes to HMX.

During the last decade, U.S. Army researchers developed a two-step process for preparing HMX that involves the intermediate production of DADN (Fig. 1d).[1-3] Both steps of this process give high yields, and the overall process is economically competitive with the current HMX process. Because the new process offers no clear advantage over the old one, however, there has been no strong incentive for investing capital in it.

The most costly and difficult step in this new process is the preparation of dinitrogen pentoxide (N_2O_5), which at present is carried out by the dehydration of HNO_3 with polyphosphoric acid ($(HPO_3)_x$):

$$(HPO_3)_x + 2HNO_3 \rightarrow H_3PO_4 + N_2O_5.$$
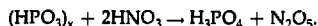
However, recycling the resulting orthophosphoric acid (H_3PO_4) back to polyphosphoric acid is very expensive. A less costly process for generating N_2O_5 would significantly reduce the cost of HMX.

Years ago, investigators in Germany and Poland reported that N_2O_5 could be produced by electrolyzing a solution of dinitrogen tetroxide (N_2O_4) in anhydrous nitric acid.[4,5] Where it is applicable, electrosynthesis has many advantages over other chemical processes: fewer side reactions, easier recovery of the pure product, and direct electrical control and monitoring of the process. Therefore, we examined this reaction using the modern technique of

controlled-potential electrolysis to assess its usefulness as an alternative to the polyphosphoric acid process.[6]

Controlled-Potential Electrolysis

Conventional electrolysis uses two electrodes, the anode and the cathode. In controlled-potential electrolysis, we add a reference electrode, the potential of which is accurately known on a standard scale, and a potentiostat to control the potential difference between the working electrode (in this case the anode) and the reference electrode (Fig. 2). Our instrumentation measures the potential of the solution with respect to the reference electrode and, hence, the potential difference between the solution and the (grounded) working electrode, which determines the nature of the electrochemical reaction. The feedback control action of the potentiostat maintains the desired potential difference between the working and reference electrodes, regardless of conditions in the electrolytic solution, by adjusting the voltage applied to the counter electrode (in this case the cathode).

In N_2O_5 synthesis. we can prevent the electrolysis of the nitric acid solvent (even after all the N_2O_4 is used up) by keeping the anode potential from going too high or too low. This maximizes the current efficiency (the percentage of the electrolysis current that performs the desired reaction) and minimizes side reactions.

Figure 3 shows the electrolysis cell used for N_2O_5 preparation. The large surface area of the platinum-screen anode facilitates the oxidation reaction. The flow of current dissipates considerable heat, making it necessary to cool the solution during electrolysis. The tube surrounding the cathode terminates in a semipermeable membrane of Vycor glass, which allows the passage of enough ions to sustain the current but prevents water formed at the cathode from reaching the anode region. The reference is a saturated calomel electrode connected to the anode solution by a salt-bridge tube filled with HNO_3.
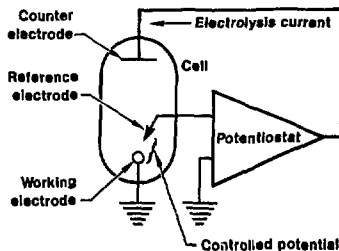
Fig. 2

Schematic diagram of the controlled-potential electrolysis system for controlling the potential between the solution and the working electrode. Current flowing from the counter electrode to the working electrode causes the desired electrochemical reaction; close control of the potential difference at the surface of the working electrode eliminates unwanted side reactions.
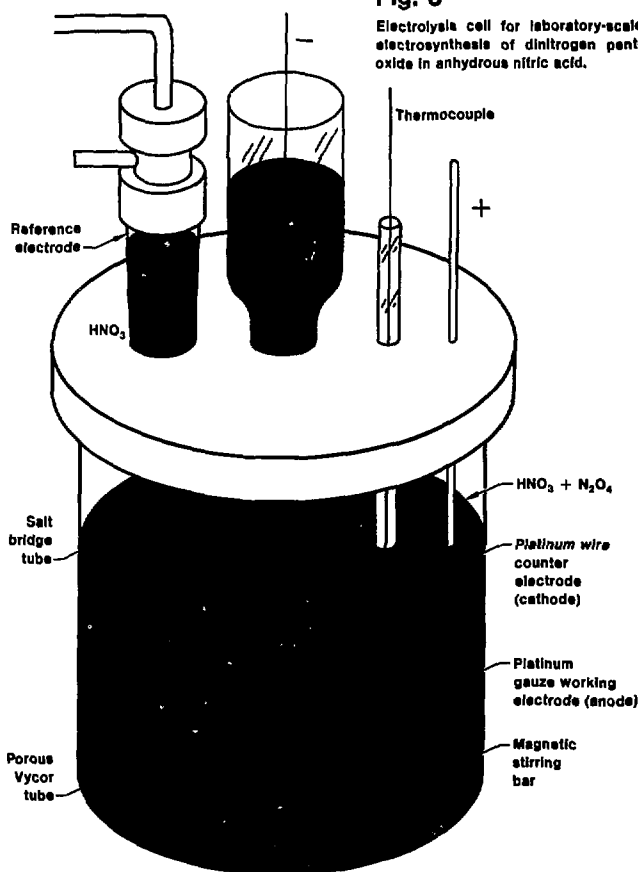
Fig. 3

Electrolysis cell for laboratory-scale electrosynthesis of dinitrogen pentoxide in anhydrous nitric acid.

13

The electrolytic synthesis of N_2O_5 in HNO_3 is an old approach whose implementation has benefited from the application of new technology.

Characteristics of the Electrolysis

The relation between current density and electrode potential in the oxidation of N_2O_4 to N_2O_5 at a platinum electrode under controlled-potential conditions is shown in Fig. 4. The region of useful potential extends from about $+1.35$ V (below which the HNO_3 solvent is reduced) to about $+1.95$ V (above which the HNO_3 is oxidized). The optimum control potential is about $+1.8$ V, corresponding to a current density of about 100 mA/cm^2.

Figure 5 shows how the current and the total cell voltage (cathode to anode) vary during an electrosynthesis. The current is nearly constant until the reaction is about 80% complete; it drops to a low background value when all of the N_2O_4 is gone.

From current vs potential curves, measured with low concentrations of N_2O_4, and the current vs time behavior of the electrolysis, we find that this oxidation of N_2O_5 is electrocatalytic. That is, the overall rate is limited, not by mass transport, but by microscopic effects on the surface of the working electrode. In this case, the surface of the electrode is a thin film of platinum oxide, which participates in the transfer of electrons (and probably of oxygen atoms) between the metal and the species being oxidized.

Characteristics of the N_2O_5 Electrosynthesis

Although the overall characteristics of this electrosynthesis are very good (high current efficiency, reasonable energy efficiency, and good yield of very pure solutions of N_2O_5 in HNO_3), the electrolysis exhibits several idiosyncrasies that are only partially understood. At first glance, one might expect, from the compounds involved and the change in oxidation number of the nitrogen, that one mole of N_2O_5 would be produced for each mole of N_2O_4 consumed and that two moles of electrons would be required. We do observe an N_2O_5:N_2O_4 ratio close to 1, but the electron requirement is variable, approaching one and a half moles at high

N_2O_4 initial concentrations. Further study reveals a complex chemical system.

Figure 6 depicts the various chemical species whose presence we have verified by Raman spectroscopy (other investigators have reported several more) and the reactions that may take place as the N_2O_4 solution is electrolyzed. Considering two of the possible anode and cathode reactions together, the sum or net cell reaction is simply the dehydration of HNO_3 to form N_2O_5:

Anode reaction:
$$N_2O_4 + 2HNO_3 \rightarrow 2N_2O_5 + 2H^+ + 2e^-$$

Cathode reaction:
$$2HNO_3 + 2H^+ + 2e^- \rightarrow N_2O_4 + 2H_2O$$
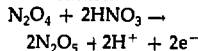
Net cell reaction:
$$2HNO_3 \rightarrow N_2O_5 + H_2O.$$
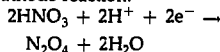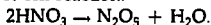
Producing HMX

We have found that solutions of N_2O_5 in 100% nitric acid from the electro-oxidation of N_2O_4 are excellent reagents for the production of HMX under a variety of conditions. The basic process involves dissolving an HMX precursor, either DADN or TAT, in the HNO_3-N_2O_5 reagent and heating it for about an hour. (In TAT, the NO_2 groups of DADN are replaced with acetyl groups.) The reaction proceeds sequentially, replacing the acetyl groups one at a time with nitronium ions (NO_2^+) from the N_2O_5.

We normally run the reaction at about 47°C, the boiling point of the HNO_3-N_2O_5 mixture, producing quite pure HMX in yields over 80%. The reaction goes faster at higher temperatures (and pressures), but the HMX produced begins to decompose, slightly decreasing the overall yield. The results are similar whether we start with DADN or with TAT.

Scaling Up the Electrosynthesis of N_2O_5

As a laboratory-scale batch synthesis procedure for producing up to 100-g
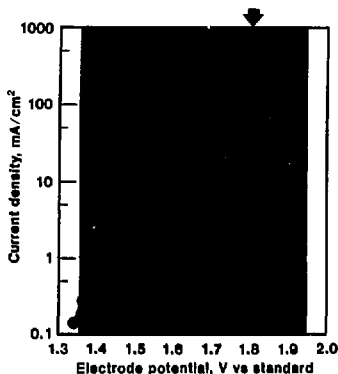
Fig. 4

Plot of current density vs electrode potential for the electrolysis of 12.5% N_2O_4 in anhydrous HNO_3 at a platinum electrode and 23°C. The broad shaded band is the operating region over which the nitric acid is neither oxidized nor reduced; the arrow indicates the optimum operating potential.

quantities of N_2O_5, the anodic oxidation of N_2O_4 to N_2O_5 is convenient, relatively inexpensive to implement, and exceptionally easy to control. As an industrial-scale process, the principal advantage of the electrosynthesis procedure would be its low cost. Although we have carried out no detailed economic analysis, the specific electrical energy consumption (the main cost of the process) appears favorable.

Further scale-up probably would entail adapting the process to a two-electrode flow cell. Refinements in cell design could lead to further cost reductions. It should be possible to devise a method to recover the N_2O_4 generated at the cathode for reuse at the anode. In addition, new materials could lower the cell voltage and hence its power dissipation.

We have made preliminary tests on several such materials, one being a perfluorinated ion-exchange membrane that could replace the semipermeable glass separator. Another is a working
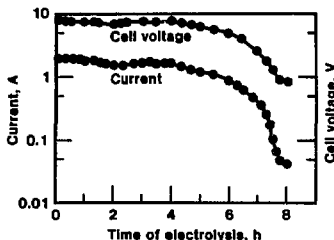
Fig. 5

Cell current and voltage during the electro-oxidation of 22.7 g of N_2O_4 in anhydrous HNO_3. The potential of the platinum working electrode was controlled between +1.78 and +1.85 V with respect to the reference electrode.

Fig. 6

Chemical species and reactions in the anode and cathode compartments of the electrolysis cell during the electrosynthesis of N_2O_5. (a) Initial solutions. (b) During electrolysis. (c) Final solutions.

(a)

Anode +   Semipermeable membrane   Cathode −

Initial solutions

(b)

Anode +   Semipermeable membrane   Cathode −

During electrolysis

(c)

Anode +   Semipermeable membrane   Cathode −

Final solutions
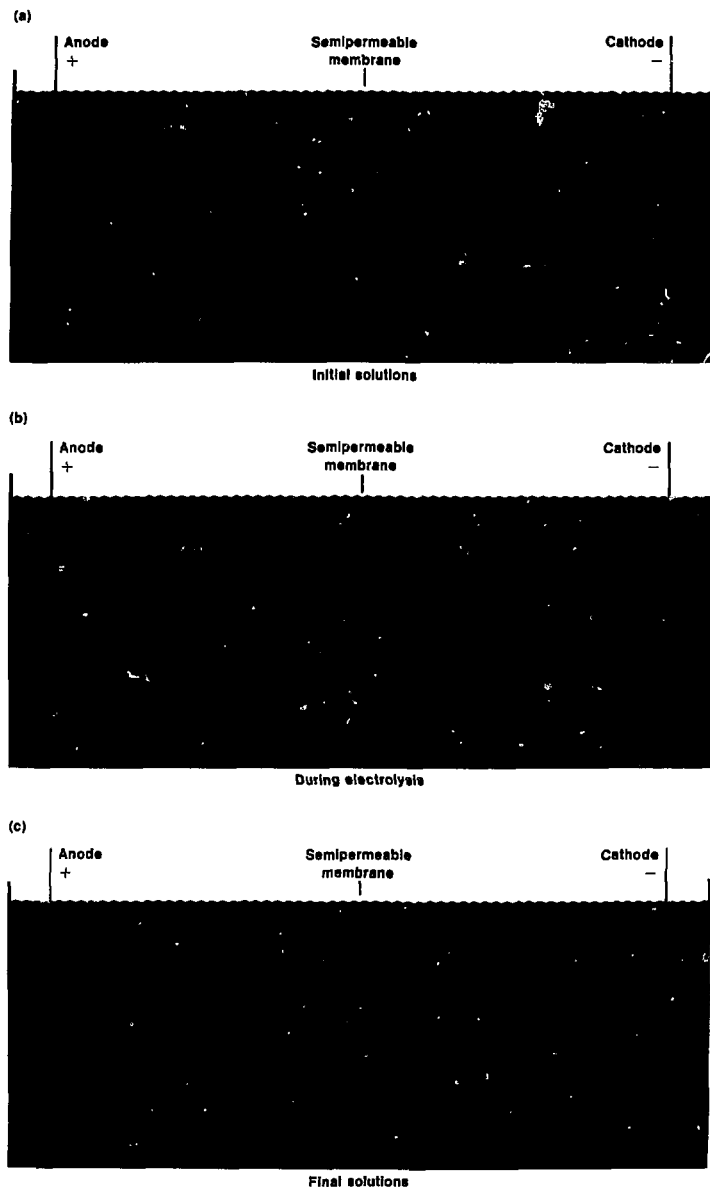
electrode made of iridium oxide coated on titanium. This material is less expensive than platinum and, at the required operating-current densities, lowers the control potential by 0.4 V.

Conclusion

The electrolytic synthesis of N_2O_5 in HNO_3 is an old approach whose implementation has benefited from the application of new technology. With the newer cell materials, which we have only briefly examined, and our recently acquired knowledge of the reaction characteristics, it should be possible to scale up the electrosynthesis of N_2O_5 and incorporate it as an economical step in the manufacture of HMX.

The production of HMX by this technique resembles the production of RDX by the Woolwich process. This means that the same basic processing equipment and reagents (N_2O_4 and HNO_3) can be used to produce either RDX or HMX without any separation or purification and without the acetic acid stream required by the Bachman process.

Notes and References

1. V. I. Siele, M. Warman, J. Leccacorvi, R. Hutchinson, R. Motto, and E. E. Gilbert, *Alternative Processes for HMX Manufacture*, U.S. Army Armament Research and Development Command, Dover, New Jersey, Rept. ARLCD-TR-78008 (1979).

2. T. M. Benziger, R. K. Hohwer, and R. K. Davey, *Process Development Studies on DADN Manufacture*, Los Alamos National Laboratory, Los Alamos, New Mexico, Rept. MIPR-5311-1029 (1976).

3. M. D. Coburn and T. M. Benziger, "Process for Producing 1,5-Diacetyl-3,7-Dinitro-1,3,5,7-Tetraazacyclooctane," U.S. Patent 3,926,953 (1975).

4. "Process for Preparation of Solutions of Nitrogen Pentoxide in Nitric Acid Monohydrate," German Patent No. 231,546 (1910).

5. J. Zawadski and Z. Bankowski, "Electrochemical Preparation of Nitrogen Pentoxide," *Roczniki Chemii* 22, 233, (1948).

6. J. E. Harrar and R. K. Pearson, *Electrosynthesis of N_2O_5 by Controlled-Potential Oxidation of N_2O_4 in Anhydrous HNO_3*, Lawrence Livermore National Laboratory, Rept. UCRL-87123, Rev. 2 (1982).
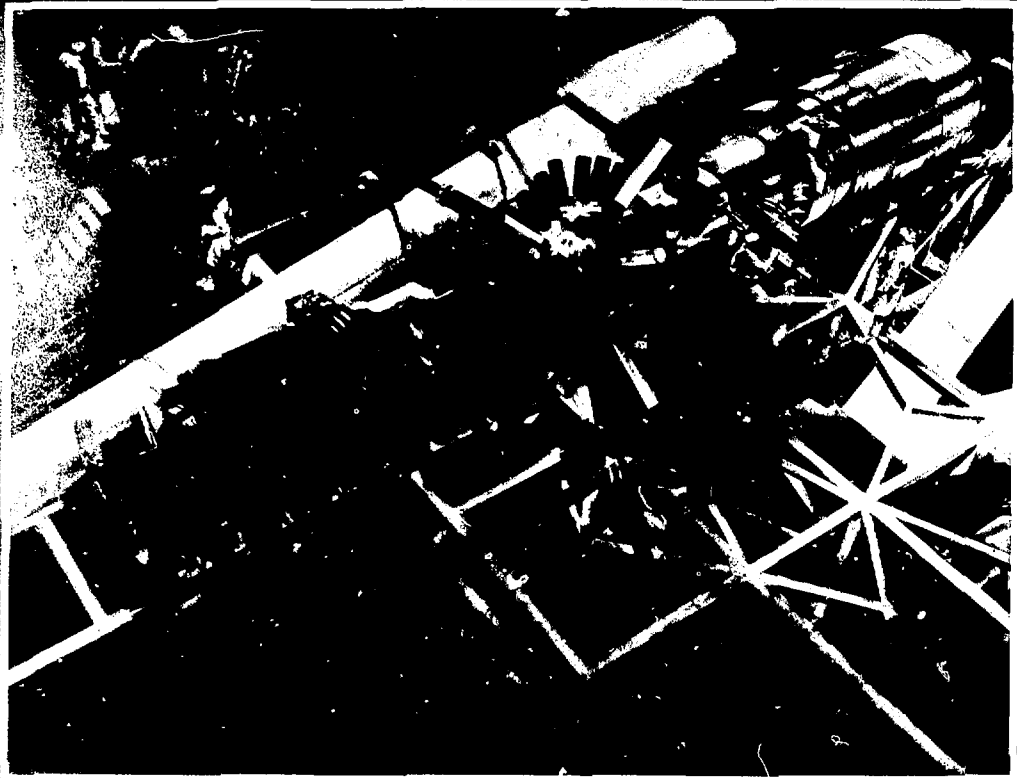
In inertial confinement fusion, tiny but powerful thermonuclear explosions are produced by focusing a laser beam on microscopic (0.1 to 5.0 mm) deuterium-tritium (D-T) targets. Because the laser beam is very intense (10^5 to 10^7 GW/cm^2), it generates a dense plama where it impinges on the target material. This plasma interacts strongly with the laser beam. Recent experiments on laser-plasma interactions have confirmed theoretical predictions that target performance improves at laser wavelengths shorter than 1 μm, the wavelength of most target-irradiation studies at LLNL.[1] This result has encouraged us to develop short-wavelength target-irradiation facilities.

The desired wavelengths can be most efficiently achieved by converting the fundamental wavelength produced by current neodymium-glass lasers. The Laboratory's Nova laser, now under construction, is a neodymium-glass system that will produce a beam of 80 to 120 kJ.[2] A frequency-conversion subsystem between the output beam and the target will enable Nova to operate at shorter wavelengths. We plan to conduct target-irradiation studies with Nova to measure quantitative improvements in target performance at wavelengths of 1.052, 0.53, and 0.35 μm. We review, here, the physics of laser-plasma interaction at shorter wavelengths and describe the frequency-conversion system to be used with Nova.

Laser-Plasma Interaction Studies

Two effects lead us to believe that the performance of directly driven fusion targets will improve at shorter wavelengths of incident laser light: the target absorbs more light, and the deleterious preheating of the fuel by fast electrons is reduced. These effects depend on the highly nonlinear physics of plasma instabilities and their excitation by an intense electromagnetic wave.

Recent experiments have studied the absorption of light in various materials as a function of intensity and wavelength.[1] The experiments revealed that

shorter wavelengths (0.53 and 0.35 μm) both increase the maximum absorption and cause more of the incident light to be absorbed at high intensities. Analysis of these results indicates that the absorption of laser light is improved because inverse bremsstrahlung is more efficient at shorter wavelengths.

Shorter wavelengths also affect preheating of the fuel in these laser-driven targets. The PdV work necessary to compress a gas such as a D-T mixture increases with the gas temperature. Therefore, any heating of the fuel before compression increases the work (i.e., the laser energy) required to compress it. High-velocity suprathermal electrons produced by collective laser-plasma interactions may preheat the target before compression by penetrating to the fuel, where they deposit their kinetic energy. Recent experiments have shown that at shorter wavelengths, the number of suprathermal electrons is reduced significantly. Thus, by reducing preheating, shorter wavelengths make another contribution to reducing the laser energy required for ignition.

Generating Shorter Wavelengths

The foregoing experimental results indicate that target performance should improve as the wavelength of the laser drive is reduced below 1 μm. There are, however, several fundamental limitations on the range of operating wavelengths for technically feasible laser systems.[3] These include the availability of a lasing medium, the effects of light propagation in optically non-linear materials, and the damaging effects of intense, short-wavelength light pulses on optical materials.

Because of these constraints, the shortest wavelength generally considered practicable for laser drivers is about 0.25 μm. In contrast, the most powerful existing target irradiation facilities use lasers that operate either near 10 or near 1 μm. As a practical matter, then, we decided to reduce the wavelength of the driver up to a factor of four. By interposing a frequency-conversion subsystem between the output ports of the laser arms and the

target, we can shorten the wavelength of the laser output. This approach has proven to be most cost effective with neodymium-glass lasers and is the one we have adopted.

Recent experiments on laser-plasma interactions have confirmed theoretical predictions that target performance improves at laser wavelengths shorter than 1 μm . . .

Frequency Conversion

In principle, any physical phenomenon that changes the frequency of light is a candidate for frequency conversion. In practice, however, other requirements limit our choice. These include:

- A focusable output (less than 20 times the diffraction-limited spot size).
- A high conversion efficiency (greater than 70%).
- A high damage threshold (above 5 J/cm^2).
- Simplicity.
- Availability of materials.

With regard to conversion efficiency, for example, there would be no cost advantage to a technique that requires a larger neodymium-glass laser facility to reach ignition with frequency conversion than without it.

To satisfy these conditions, frequency conversion must be based on a physical phenomenon that is coherent, saturable, and virtually lossless. Among such phenomena are stimulated multiphoton Raman scattering, the generation of a sum frequency by two-, three-, or four-wave mixing, and the generation of harmonics in optically nonlinear media. Each of these has its own impact on laser system design. Where the input for the conversion process requires waves of different frequency, the effect on the laser system is considerable. We have decided to use harmonic conversion in nonlinear

media, which requires no auxiliary inputs and thus has the virtue of simplicity and economy. This process is the best understood frequency-conversion technique and also provides the most control over the beam quality of the converted light.

Harmonic Generation

Harmonic-conversion techniques are well understood and are routinely implemented in small-aperture commercial lasers.[4] Very intense laser light incident on a transparent medium interacts with the material's atomic structure to generate electromagnetic radiation with frequencies that are multiples of the fundamental frequency of the incident light, ω (see box on p. 22). These are known as harmonics of the fundamental frequency. The strongest of these is at 2ω, and the next strongest is at 3ω. For high conversion efficiency, the phase velocities of the waves must be commensurate; the process that achieves this is called phase matching. Phase-matched conditions generate high-power harmonics of the fundamental wave that have a focal spot approximately the same size of that of the fundamental wave.

In negative uniaxial crystals such as potassium dihydrogen phosphate (KDP), we can phase match in one of two ways (called type I and type II), depending on the orientation of the polarization of the waves relative to the crystal axis and to the direction of propagation (see box on p. 22). Phase matching thus requires precise orientation of the crystals. Our design for a KDP frequency-conversion subsystem uses type-II phase matching and a novel arrangement of the crystals to provide maximum flexibility for the laser system.

KDP as a Conversion Medium

Many materials exhibit the properties needed for frequency conversion. The most commonly used are the crystalline solids potassium dihydrogen phosphate (KDP), ammonium dihydrogen phosphate (ADP), and their deuterated isomorphs. These materials also have

the properties, listed above, essential to the fusion application. (We considered other materials, such as atomic vapors, vapors of asymmetric molecules, and various solid and liquid media; none, however, proved as readily adaptable to the neodymium-glass laser.)

KDP was the first material found to exhibit phase-matched generation of the second harmonic.[5] Although the number of such materials has since climbed into the hundreds, KDP remains a primary choice. During the 1970s, the development of KDP for use in Pockels cells (a type of optical switch) led to the production of crystals of excellent optical quality with a clear aperture approaching 10 cm in diameter. Major crystal growers are continuing their efforts to increase aperture diameter, now emphasizing the undeuterated form. Undeuterated KDP crystals have an optical quality superior to the deuterated form, do not require as expensive a growth facility, and have provided most of the growers' experience.

Compared with other candidate materials, KDP is resistant to laser-induced damage, has an adequately high harmonic-generation coefficient and a very low self-focusing index, and transmits ultraviolet frequencies well. It can be grown from solution to unusually large sizes and can be phase matched to generate 2ω, 3ω, and 4ω harmonics from 1.064- or 1.053-μm light (actual fundamental wavelength is a function of the specific glass used in the neodymium-glass laser). These properties outweigh KDP's relative disadvantages, which include undesirable absorption (0.058/cm) at 1.064 μm, its softness and consequent polishing difficulty, significant hygroscopicity, susceptibility to fracture, and slowness of crystal growth (about 1 mm a day).

Several of the candidate materials are superior to KDP in at least one category. At present, however, KDP remains the only material that satisfies all the fundamental requirements of harmonic generation at 1.064 and 1.053 μm and can be grown in crystals of an adequate size in time for installation in the Nova laser. If only the second

harmonic is required, another attractive candidate material is CDA (cesium dihydrogen arsenate). Phase matching is much easier with CDA than with KDP, so long as the crystal temperature is well controlled. We are continuing to examine other candidates for future laser systems to increase system flexibility and to decrease the cost of the frequency-conversion subsystem.

Frequency Conversion in Novette and Nova

The Laboratory first applied KDP crystals to harmonic conversion with its Argus laser. With both the upgraded Argus (Novette) and the high-power Nova neodymium-glass lasers, we will use KDP to generate second and third harmonics for studies of the irradiation of fusion targets. Our objective is to convert the infrared (1.053-μm) light produced by these lasers to visible green (0.53-μm) or blue (0.35-μm) light. This conversion entails five major design requirements:

- High conversion efficiency from the fundamental frequency to the second and third harmonics.
- Harmonic generation with a large (74-cm) aperture.
- Multiwavelength flexibility at minimum cost.
- Integration with the target alignment and diagnostics systems.
- Minimization of nonlinear propagation effects.

Conversion Efficiency

Conventional methods of generating the second and third harmonics tend to work efficiently over a limited intensity range. Applied to Nova, such methods would require three interchangeable crystal arrays, each with a different crystal thickness, to achieve the desired performance over a wide range of input intensities. We have developed a system capable of generating the second and third harmonics over the required intensity range using only a single array containing two crystals. Our design is called the quadrature-green/cascade-blue scheme.[6]

To generate the third harmonic, we use two crystals already in the basic

Harmonic Generation in KDP

When a low-intensity light wave propagates through a transparent medium, it drives the electron cloud of the constituent atoms into forced oscillation (a). This oscillating electric charge constitutes a polarization wave that gives rise to a radiated wave. The radiated wave represents the usual "linear" response of the medium to the incident light. Because the oscillatory motion of the electrons follows the vibratory motion of the driving field, the radiated wave is of the same frequency as the incident wave. The wave thus emerges from the transparent medium with its frequency unchanged but with a phase delay that depends on the material's refractive index. This applies to all low-intensity light waves passing through transparent media.

Laser pulses typically have a spectral brightness (power density per steradian-hertz) many orders of magnitude greater than that of incoherent sources. It is this property that enables a laser pulse to produce a more vigorous oscillation of the electron cloud. The electrons may be displaced from their equilibrium position by a distance many times larger than the truly minute excursion induced at low intensity. As a result, the electrons come into greater contact with neighboring atoms, probing their repulsive potential with each oscillatory cycle. This process enables the structure of the medium to influence the frequency of light radiated by the oscillating electrons. If the strength of the repulsion experienced by an electron driven by intense laser light is asymmetric (different in opposite directions), its motion will be biased (b).

If we decompose an electron's motion into its frequency components, they appear at multiples of the input frequency, ω (c). For a centrosymmetric site, the components appear at odd multiples (mostly 3ω and, to a vastly smaller extent, 5ω). For an asymmetric

site, we obtain both odd and even multiples. By far the strongest of these is 2ω and, in order of rapidly decreasing strength, 3ω, 4ω, and higher frequencies. (There is also a zero-frequency, or dc, polarization term). Each of the oscillatory motions gives rise to a radiated wavelet (a harmonic) at multiples of the input frequency.

In generating second harmonics, for example, each wavelet at the second harmonic frequency, 2ω, radiates outward at the phase velocity of the medium for that frequency, which is the vacuum speed of light divided by the refractive index at 2ω ($v_{2\omega} = c/n_{2\omega}$). The fundamental wave, however, propagates with a different phase velocity ($v_\omega = c/n_\omega$). Because the fundamental wave imposes its phase on each of the electron oscillators, and thus on the radiated 2ω wavelets, the net radiated wave at 2ω is the sum of many out-of-phase wavelets from the host of oscillators throughout the material. We describe this situation by saying that the process is not phase matched (d). The result is a very weak conversion of the laser energy from the fundamental to the desired frequency, 2ω.

To achieve the phase-matched condition, in which the 2ω wavelets will add coherently, we must arrange for the phase velocity of the fundamental wave to equal that of the second-harmonic wave. This can be done by choosing a material with anisotropic characteristics that compensate for the variation in phase velocity with wavelength. The wavelets from all the oscillators in such a material then will reinforce one another (d), resulting in a high conversion efficiency. KDP crystals display this property.

The phase velocity of light in a transparent medium is inversely proportional to its refractive index, which, in turn, depends on the spatial orientation of the material and on the wavelength of the light. It is possible to orient a crystal of KDP so that the propagation velocity of incident light waves produces exact phase matching.
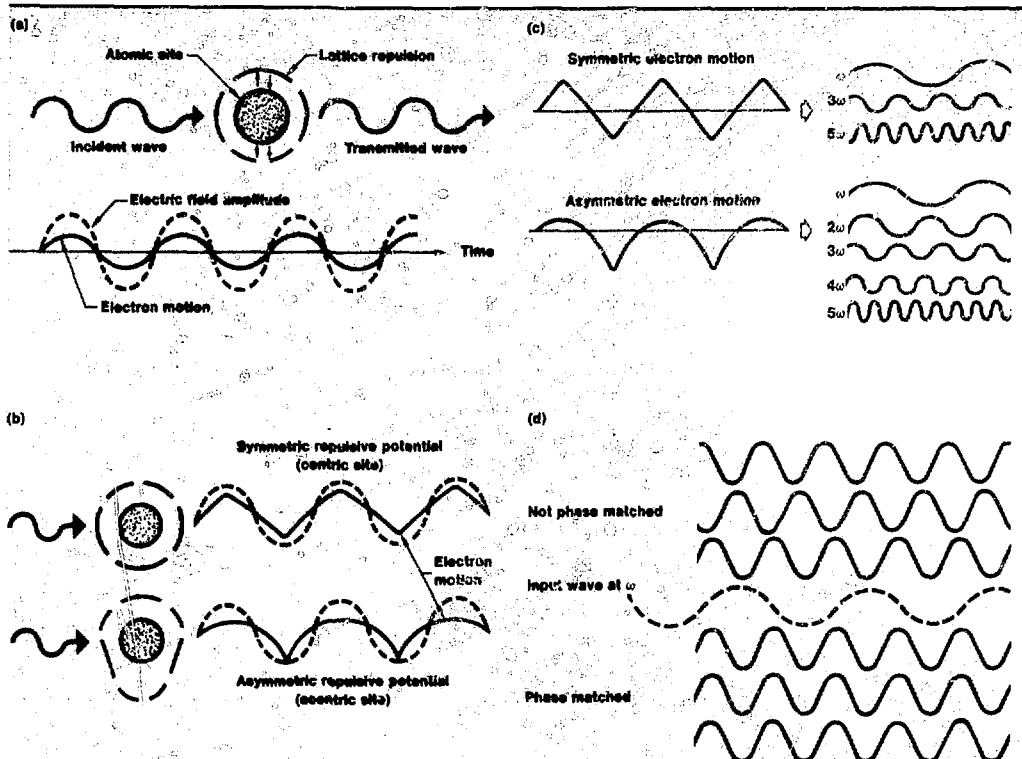
The optical axis of KDP is such that light polarized perpendicular to the axis experiences an angle-independent (ordinary) refractive index, n_o, whereas light of the other polarization experiences an angle-dependent (extraordinary) refractive index, n_e (e). The extraordinary index $n_e(\theta)$ at the second harmonic is equal to the ordinary index at the first harmonic at a particular angle θ, the phase-matching angle of incident light. This condition, called type-I phase matching, produces phase matching for the second harmonic.

Phase matching may also occur when the second harmonic is matched with two fundamental waves polarized in orthogonal directions.[4] This is called type-II phase matching. In this way, a KDP crystal provides a high conversion efficiency in one particular orientation but a low efficiency in any other orientation. We have demonstrated experimentally this conversion technique, called angle-tuned harmonic generation, with the Laboratory's Argus and other laser facilities. This technique requires precise orientation of the KDP crystal, typically to within 100 μrad.

23
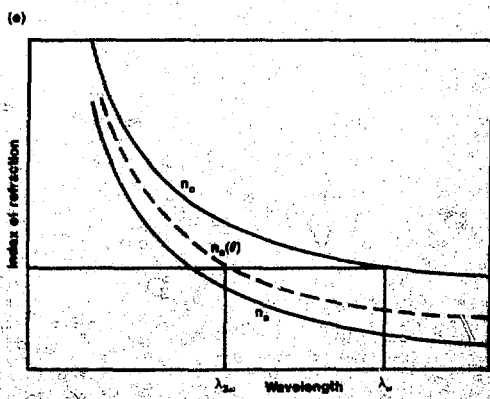
orientation for generating blue (0.355-μm) light.[7,8] This is the standard cascade-blue configuration. For high conversion efficiency, we optimize the crystal lengths for efficient performance over the full operating range of input intensity. To generate the second-harmonic green (0.532-μm) light, we have developed a new approach, the quadrature scheme (see box on p. 26). In this scheme, two crystals are arranged almost exactly as in the cascade-blue configuration. To change the system from generating blue to generating green light, we need only rotate the two-crystal array about the beam axis by 10 deg and angle-tune the second crystal (about only one axis of the assembly) from the blue phase-matching angle to the green phase-matching angle—a rotation of just a few milliradians. In contrast to conventional approaches, there is no need for interchangeable arrays.

Our scheme produces green light efficiently over a large operating range of input intensity, much larger than the system requirement (Fig. 1). It performs best at the low-intensity end of Nova's pulse-width range (2 to 5 ns). This design is consistent with other system constraints such as minimizing nonlinear propagation effects.

Large-Aperture Arrays

Nova requires frequency-conversion arrays with a large (74-cm) aperture. The feasible aperture size of single KDP crystals is limited, at present, as large-aperture crystals have a high aspect ratio (aperture divided by thickness) and a long fabrication time. This limitation can be overcome, however, by fabricating an array of small-aperture crystals to provide a large total aperture. We have used this technique in designing the frequency-conversion subsystem for Nova. In our two-crystal subsystem, each 74-cm aperture is fabricated of nine KDP segments (Fig. 2). Each array is sandwiched between two windows coated with graded-index antireflection layers.[9] Losses from Fresnel reflections at surfaces inside the assembly are reduced with three thin layers of index-matching fluid. The composite arrays are assembled by precisely machining the KDP crystals so that the phase-matching direction (the beam direction) is accurately aligned with the surface normal. This approach was made feasible by the use of diamond-turning technology to machine the crystals and by precise measurement of the phase-matching angle (± 30 μrad).

Exacting requirements for the optical quality of the beam severely constrained the mechanical design of the assembly. We developed and tested two designs using a 15-cm, clear-aperture prototype. In the "egg crate" design, the crystals are embedded in a stainless-steel lattice that supports the windows against an internal vacuum load. We have also tested a "close packed" design, in which the individual crystal segments are placed directly against each other, and the whole array is supported by the windows and perhaps some internal post supports. (Experimental results from a prototype close-packed array are shown in Fig. 3.) We are evaluating, both experimentally and theoretically, the relative merits of these two designs.

The intensity of high-power lasers is limited by self-focusing, a phenomenon whereby small-amplitude, small-scale intensity ripples in the laser beam amplify to very high intensities that can damage optical components.[3,10,11] This effect, caused by nonlinearities in the optical materials, occurs to some extent in all optical components, including the target-focusing optics. The severity of

Fig. 1

Calculated conversion efficiency of the quadrature-green/cascade-blue arrangement, assuming a Nova whole-beam divergence of 200 μrad and the optimum crystal thickness of 1.4 cm for both crystal arrays. (a) The conversion efficiency ($\eta_{2\omega}$) of the fundamental harmonic (ω) to green light (the second harmonic) is high over the full operating range (0.5 to 3 GW/cm²); (b) the efficiency of conversion ($\eta_{3\omega}$) to blue light, (the third harmonic) declines at higher intensities of the fundamental frequency. Efficient conversion to blue light is not necessary beyond 2.5 GW/cm², as the intensity of the incident laser beam is limited by self-focusing in the target-focusing optics.

Conversion efficiency vs. Incident Intensity (fundamental wavelength), GW/cm². Curves labeled "Second harmonic" and "Third harmonic."
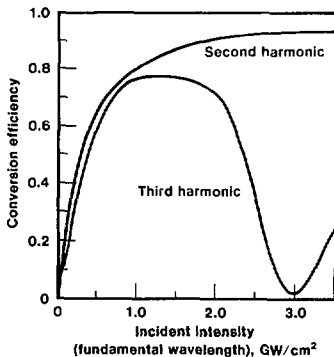
the effect increases with the optical path length and with the laser intensity and decreases with wavelength. Segmented crystal arrays induce ripples in the beam when it is diffracted by the gaps between segments, subjecting it to self-focusing in the target-focusing optics, especially at the third harmonic (0.35 μm). In our design, we minimize rippling by using apodization to control diffraction from the gaps (apodization is a method of softening hard edges that clip the beam).

Design of the Frequency-Conversion Subsystem

The conversion scheme produces two wavelengths by using the same arrays that generate the second harmonic to generate the third harmonic; the color is changed merely by adjusting the orientation of the arrays. The rest of the frequency-conversion subsystem is designed to be similarly color flexible.

Components of high-power lasers typically perform best (in terms of damage threshold, reflectivity, and wavefront distortion) when they are optimized for monochromatic operation. It is not economically feasible, however, to use, say, three sets of 74-cm-aperture focusing optics, one for each operating wavelength. Therefore, we designed the frequency-conversion and target-focusing subsystems to operate at multiple wavelengths, minimizing the number of multiwavelength components. Furthermore, the total

path of the laser beam through glass is minimized so as to maximize the highest power at which the laser operates without undergoing self-focusing.[6]

The spatially filtered infrared laser beam produced by each arm of Nova is imaged onto the target-focusing optics through a system of mirrors that are
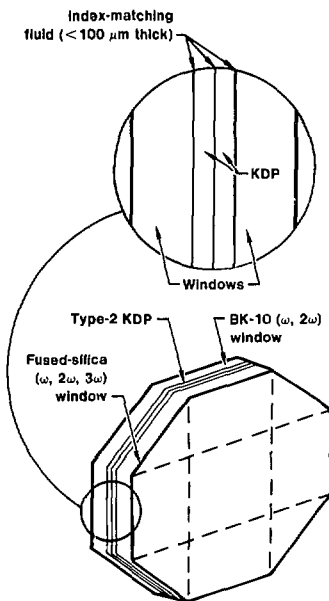
Fig. 2

Each 74-cm frequency-conversion aperture is fabricated of nine KDP segments. The three-by-three array is sandwiched between two anti-reflecting windows. Losses from Fresnel reflections at surfaces inside the assembly are reduced with three thin layers of index-matching fluid. The KDP crystals are machined so that the phase-matching direction (the beam direction) is accurately aligned with the surface normal.

Fig. 3

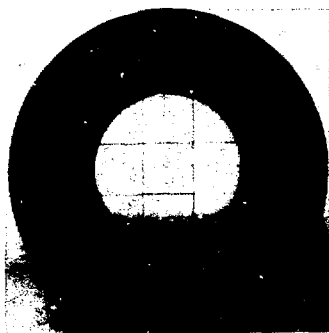Using a prototype close-packed KDP crystal array (left), we were able to generate the second-harmonic green light (right). Data were taken with the Argus laser facility: laser output at 1.064 μm and 0.7 ns was 2 GW/cm^2; crystal width was 5 cm; crystal thickness was 11.8 mm. The measured conversion efficiency from the fundamental infrared wavelength to the second harmonic (green) was 75%.

25

(a)
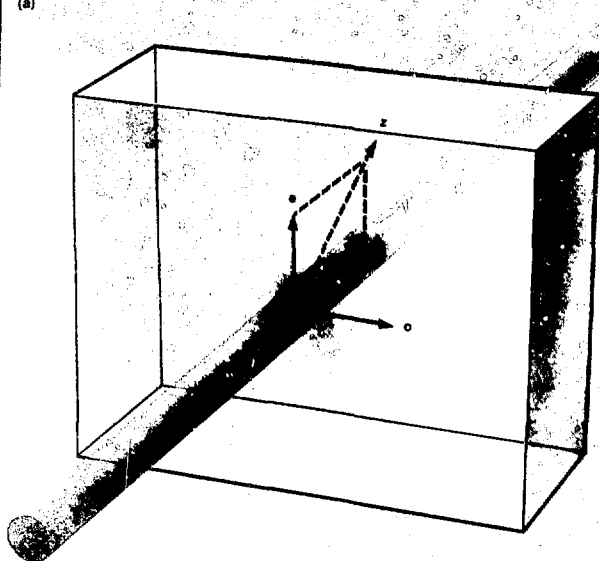
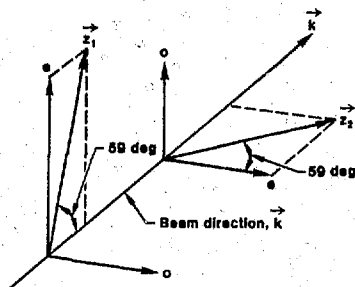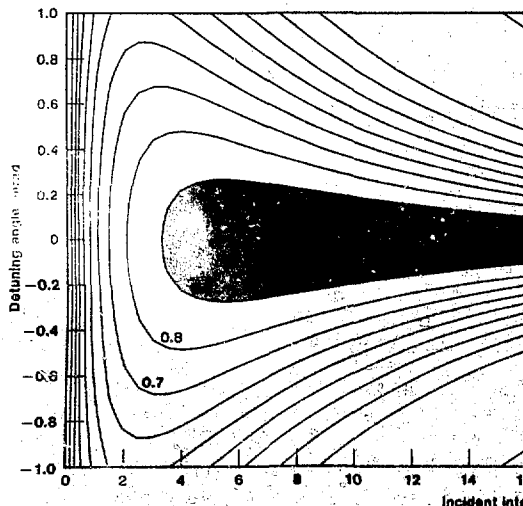## Quadrature Conversion Scheme

The quadrature conversion scheme is a method of generating the second harmonic of a fundamental wave. The scheme, which uses two crystals in series, has several advantages over single-crystal or other two-crystal schemes:
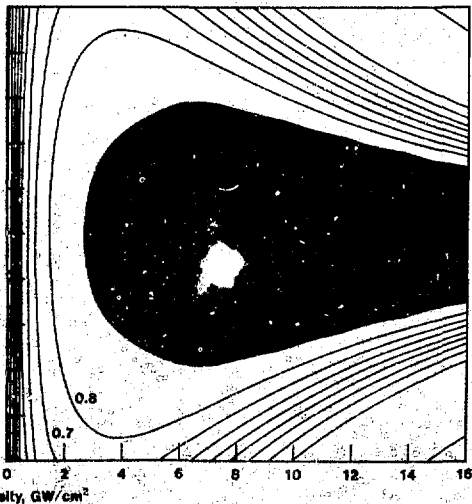
(b)

59 deg

59 deg

Beam direction, $\vec{k}$

(c)

(d)

Detuning angle, rad

Incident intensity, GW/cm²

0.8

0.7

0.8

0.7

- High conversion efficiency over a large dynamic range of drive intensity and detuning angle.
- Easier crystal alignment.
- The same crystal configuration as the two-crystal methods of generating the third harmonic, making the transition from a 2ω to a 3ω output much simpler.

Consider a pair of KDP crystals cut for type-II phase matching [in (a) we show the first crystal of the pair]. In the quadrature scheme, the optical axes of the crystals are arranged so that the planes containing the direction of the laser beam and their optical axes (the kz planes) are mutually perpendicular (b). This arrangement has two important properties. First, in type-II phase matching, the incident wave is polarized at 45 deg to the kz plane of the crystal. Thus, in the quadrature scheme, if the incident wave is correctly polarized for efficient conversion in the first crystal, it is also correctly polarized for efficient conversion in the second crystal (b). Both crystals can therefore convert efficiently.

Second, the second harmonic waves generated in the two crystals are orthogonally polarized (hence the term quadrature). The output from the first crystal thus has the wrong polarization to experience gain in the second crystal. If the conversion efficiency is η_1 in the first crystal and η_2 in the second, the output from the first crystal is $\eta_1 I$ (where I is the incident intensity of the fundamental wave) and the input intensity to the second crystal is $(1 - \eta_1)I$. Because the second crystal does not change the output of the first, the overall output is simply the sum of the output from each crystal. The overall conversion efficiency is then

$$\eta = \eta_1 + \eta_2 (1 - \eta_1) .$$

The advantage of quadrature conversion is that it enables us to arrange for the second crystal to convert whatever light is left unconverted from the first crystal.

The conversion properties of a single crystal of KDP 1.4 cm thick are plotted as contours of constant conversion efficiency in (c). Consider a large-aperture laser beam incident on the crystal. Because of the unavoidable slight aberrations present in any laser beam, the intensity and local direction of the beam (angular detuning) will vary over its face. As the crystal acts locally in converting the laser light to the second harmonic, the conversion efficiency varies from point to point over the face of the beam. The relevant conversion efficiencies are defined, therefore, by the range of intensities and angular detunings present in the beam. This range defines an area on the detuning-intensity plot. For efficient conversion, the efficiency within that region must be high. Clearly, any energy in the laser beam that meets the crystal with an intensity and detuning for which the conversion efficiency is low will remain unconverted. For efficient operation, the crystals thus must convert efficiently over a sufficiently large area in the intensity-detuning plane. The required size of this area depends on the quality of the incident laser beam. As shown in (c), a single 1.4-cm crystal converts efficiently in a roughly rectangular region (defined by the 90% contour) 200 to 400 μrad wide from 4 up to about 20 GW/cm². Any laser light falling in this region will be converted to the second harmonic with an efficiency greater than 90%.

Figure (d) shows the same plot for two 1.4-cm crystals arranged in quadrature (see b). In this case, the 90% contour occupies a much larger region—about 1 mrad wide at 6 GW/cm² and falling to 0.5 mrad wide at 15 GW/cm². The quadrature system is clearly much more forgiving of beam aberrations than is a single crystal. For the beam quality expected from Nova, angular detunings are not expected to exceed 0.2 mrad. In this case, the quadrature system gives a conversion efficiency greater than 80% for intensities above 2 GW/cm².

highly reflective at the beam's fundamental wavelength (Fig. 4). In our design, the two frequency-conversion arrays, operating in series, are placed between the last turning mirror and the focusing optics in each arm. This allows us to miminize the number of components required to perform under high-power incident light at more than one wavelength.

The multiwavelength portion of the system includes the focusing optics, debris shields, a vacuum barrier, and beam dumps. Of these, only the beam dumps are wavelength unique: these absorh the undesired residual fundamental (1.052-μm) or harmonic (0.53-μm) wavelengths. Changing the wavelength of the laser output thus requires only a slight reorientation of the crystal arrays, a minor repositioning of the target-focusing optics, and replacement of the beam dumps. Because no major components need be replaced, the system is thus highly color flexible.

The first element of the aspheric, f/6 focusing lens serves as a vacuum barrier (Fig. 4). The second element is an

f/13 aplanatic lens with the last surface uncoated. Combined, these two lenses provide an f/4 focusing system with a 4% reflection of the harmonic wavelengths for diagnostic purposes. The reflection is focused and returned to a diagnostic sensor via the same turning-mirror system that transports the beam to the arrays. By changing the spacing between the two lens elements, we can control the convergence on the diagnostic reflection to accommodate arm-to-arm variations in the distance from the lens to the sensor. This spacing change also helps compensate for the focal shift in the target plane due to dispersion in the glass.

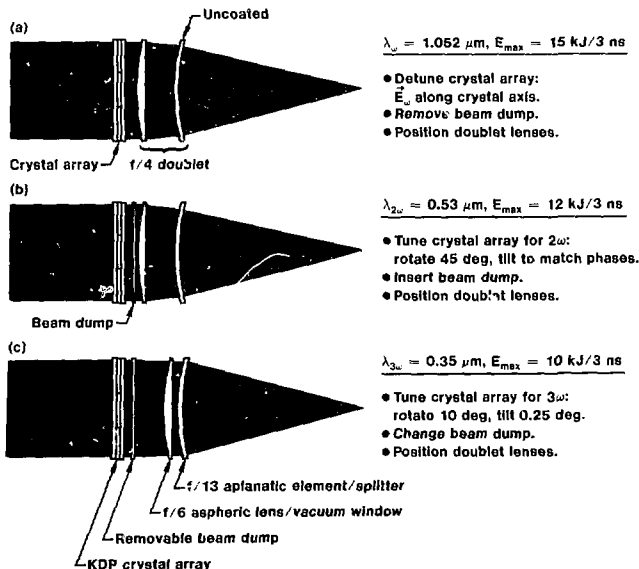## Integration of Diagnostic and Alignment Systems

The harmonic wavelengths partially reflected from the focusing-lens system are transported by the turning mirrors to a diagnostic sensor (about 30 m away). The sensor is located behind the first turning mirror in an area shielded from electromagnetic interference and from neutrons produced by fusion reactions. As the intensity of the reflected beam is low (less than 4% of the harmonic intensity) but overly energetic for diagnostic purposes, the mirrors need be neither highly damage resistant nor highly reflective at the second and third harmonics. The reflected signal is used for calorimetry and for spatial and temporal measurements.

The alignment procedure can be considered in two parts. The first is alignment of the turning mirrors and focusing optics to enable the high-power harmonic pulse to properly illuminate the target. The second is alignment of the crystal array in the phase-matching direction for efficient harmonic conversion of the incident fundamental pulse.

To align the optical elements of the system at the target, we need to know the beam direction. This is provided by low-power reference beams that are colinearly aligned with the main (high-power) laser beam. For experiments using infrared (1.052-μm) light, we will use the system alignment laser, an infrared reference beam designed into Nova. To align the optics for

Fig. 4

Frequency-conversion subsystem of Nova, showing KDP crystal positioning and target-focusing optics. Legends show the operations necessary to set the subsystem for (a) red, (b) green, or (c) blue light. The conversion wavelength can be changed without replacing major components.

(a)

Uncoated

Crystal array — f/4 doublet

$\lambda_\omega = 1.052\ \mu$m, $E_{max} = 15$ kJ/3 ns

● Detune crystal array:
  $\vec{E}_\omega$ along crystal axis.
● Remove beam dump.
● Position doublet lenses.

(b)

Beam dump

$\lambda_{2\omega} = 0.53\ \mu$m, $E_{max} = 12$ kJ/3 ns

● Tune crystal array for 2ω:
  rotate 45 deg, tilt to match phases.
● Insert beam dump.
● Position doublet lenses.

(c)

$\lambda_{3\omega} = 0.35\ \mu$m, $E_{max} = 10$ kJ/3 ns

● Tune crystal array for 3ω:
  rotate 10 deg, tilt 0.25 deg.
● Change beam dump.
● Position doublet lenses.

f/13 aplanatic element/splitter
f/6 aspheric lens/vacuum window
Removable beam dump
KDP crystal array

experiments with green (0.53-μm) or blue (0.35-μm) light, we will use an ancillary low-power, continuous-wave laser operating at the same wavelength as the desired harmonic. The ancillary laser is colinearly aligned with the system-alignment laser, thereby providing a low-power reference source of the desired wavelength. The turning mirrors and focusing optics are then positioned using standard target-alignment techniques.

To align the crystal arrays, we use the master oscillator pulse train (operating at the fundamental frequency), amplified by small-aperture rod amplifiers with a high repetition rate (0.1 Hz). We then orient an array so that it converts the second harmonic with maximum efficiency as monitored in the target chamber. This technique, however, will not produce a measurable third-harmonic signal. We align the array for the third harmonic by an open-loop correction of its position at the second harmonic. This amounts to a tilt of 4.4 mrad about one axis of the array.

Summary and Conclusions

Both theory and experimental results indicate that the performance of inertial-confinement fusion targets can be substantially improved by operating the driving laser at wavelengths shorter than 1 μm. The most efficient way of attaining wavelengths that are three to four times shorter than the current operating wavelength is by converting the laser's fundamental frequency. We have designed a frequency-conversion subsystem using multicrystal arrays of KDP. When installed with the Nova and Novette lasers, the system will operate at the second (0.53-μm) or third (0.35-μm) harmonic of the fundamental frequency (1.052 μm). The operating wavelength can be easily changed. The system should achieve high conversion efficiency and will accommodate nonlinear propagation effects over the intensity range of interest. Requirements for aligning the system and for diagnosing target performance can be met at all three wavelengths without compromising the multiwavelength flexibility.

The payoff of such a conversion system in improved target performance promises to be considerable, and KDP crystal array technology is currently sufficiently advanced to meet Nova specifications. Accordingly, plans are for the Novette laser (in late 1982) and the Nova laser (in 1984 or 1985) to provide high-energy, short-wavelength target irradiations.

Notes and References

1. Recent work at LLNL was described in the *Laser Program Annual Report*, Lawrence Livermore National Laboratory, Rept. UCRL-50021-81 (1981), Sec. 6.

2. The design and operating principles of the Nova laser were described in *Energy and Technology Review* (UCRL-52000-80-12), December 1980, p. 1.

3. J. R. Holzrichter, D. Eimerl, E. V. George, J. B. Trenholme, W. W. Simmons, and J. T. Hunt, *High Power Lasers for Fusion*, Lawrence Livermore National Laboratory, Rept. UCRL-86161 (1980).

4. F. Zernike and J. E. Midwinter, *Applied Nonlinear Optics* (Wiley Interscience Publications, New York, 1973).

5. P. A. Franken, A. E. Hill, C. W. Peters, and G. Weinreich, "Generation of Optical Harmonics," *Phys. Rev. Lett.*, **7**, 118 (1961).

6. M. A. Summers, L. G. Seppala, F. Reinecker, D. Eimerl, and B. C. Johnson, "A Two-Color Frequency Conversion System for High-Power Lasers," presented at CLEO '81, Washington, D.C., June 10–12, 1981.

7. W. Seka, S. D. Jacobs, J. E. Rizzo, R. Boni, and R. S. Craxton, "Demonstration of High-Efficiency Third Harmonic Conversion of High-Power Nd-Glass Laser Radiation," *Opt. Commun.*, **34**, 469 (1980).

8. R. S. Craxton, "Theory of High-Efficiency Third Harmonic Generation of High-Power Nd-Glass Laser Radiation," *Opt. Commun.*, **34**, 474 (1980).

9. The principles and fabrication of graded-index antireflection surfaces were described the March 1982 issue of *Energy and Technology Review* (UCRL-52000-82-3), p. 9.

10. E. S. Bliss, J. T. Hunt, P. A. Renard, G. E. Sommargren, and H. J. Weaver, "Effects of Nonlinear Propagation on Laser Focusing Properties," *IEEE J. Quantum Electron.*, **QE-12** (7), 71 (1976).

11. J. T. Hunt, W. W. Simmons, R. Speck, W. Warren, and D. Eimerl, *Beam Propagation in the Frequency Converted Subsystems of Nova and Novette*, Lawrence Livermore National Laboratory, Rept. UCID-19086 (1981).

Past Titles

Articles published in recent issues of the *Energy and Technology Review* are grouped below mainly according to their chief sponsors, the Assistant Secretaries of the U.S. Department of Energy. Research funded by other Federal agencies is listed under Work for Others.

ENERGY RESEARCH

Successful MFTF-B Technology Demonstration (Brief—May 1982)
Composite-Material Flywheels and Containment Systems (March 1982)

DEFENSE PROGRAMS
Inertial Fusion

Measuring Microsphere Targets for Fusion Experiments (June 1982)
Damage-Resistant Antireflection Surfaces for High-Power Lasers (March 1982)
Measuring the Microtopography of Optical Surfaces (March 1982)

Military Application

New Cable Emplacement Device Tested (Brief—June 1982)
The Raman Spectroscopy Microprobe (June 1982)
Slow Positrons from the 100-MeV Linac (Brief—April 1982)
The Geology of Yucca Flat (April 1982)

LABORATORY HISTORY

Thirty Years Ago: Controlled Thermonuclear Reactions (June 1982)

LABORATORY REVIEWS

Energy and the Environment (July 1982)
LLNL 1982: Technical Horizons (July 1982)
National Defense (July 1982)
Supporting Technologies (July 1982)
The State of the Laboratory (July 1982)
U.S. Oil Supply Reflects World Events (Brief—May 1982)

WORK FOR OTHERS
Department of Defense

Improving Tank Track Pads (May 1982)

Environmental Protection Agency

Atmospheric Ozone: Zeroing In (May 1982)

National Institutes of Health

Slit-Scan Flow Cytometry: A Promising New Cytometric Tool (April 1982)

Nuclear Regulatory Commission

Nuclear Waste Storage: Evaluating the Uncertainties (May 1982)
Earthquake Safety of Nuclear Power Plants (April 1982)